The Rod Domain of NF-L Determines Neurofilament Architecture, Whereas the End Domains Specify Filament Assembly and Network Formation

Susanne Heins,* Philip C. Wong,‡ Shirley Müller,* Kenneth Goldie,* Don W. Cleveland,‡§ and Ueli Aebi*‖

*M. E. Müller Institute at the Biocenter, University of Basel, CH 4056 Basel, Switzerland; and ‡Department of Biological Chemistry, §Department of Neuroscience, and ‖Department of Cell Biology and Anatomy, Johns Hopkins University School of Medicine, Baltimore, Maryland 21205

Abstract. Neurofilaments, assembled from NF-L, NF-M, and NF-H subunits, are the most abundant structural elements in myelinated axons. Although all three subunits contain a central, α-helical rod domain thought to mediate filament assembly, only NF-L self-assembles into 10-nm filaments in vitro. To explore the roles of the central rod, the NH_2-terminal head and the COOH-terminal tail domain in filament assembly, full-length, headless, tailless, and rod only fragments of mouse NF-L were expressed in bacteria, purified, and their structure and assembly properties examined by conventional and scanning transmission electron microscopy (TEM and STEM). These experiments revealed that in vitro assembly of NF-L into bona fide 10-nm filaments requires both end domains: whereas the NH_2-terminal head domain *promotes* lateral association of protofilaments into protofibrils and ultimately 10-nm filaments, the COOH-terminal tail domain *controls* lateral assembly of protofilaments so that it terminates at the 10-nm filament level. Hence, the two end domains of NF-L have *antagonistic* effects on the lateral association of protofilaments into higher-order structures, with the effect of the COOH-terminal tail domain being *dominant* over that of the NH_2-terminal head domain. Consideration of the 21-nm axial beading commonly observed with 10-nm filaments, the approximate 21-nm axial periodicity measured on paracrystals, and recent cross-linking data combine to support a molecular model for intermediate filament architecture in which the 44–46-nm long dimer rods overlap by 1–3-nm head-to-tail, whereas laterally they align antiparallel both unstaggered and approximately half-staggered.

NEUROFILAMENTS (NFs),[1] composed principally of the three polypeptides NF-L (apparent M_r 68 kD), NF-M (apparent M_r 160 kD), and NF-H (apparent M_r 200 kD), are a major component of the neuronal cytoskeleton (for a review see Liem, 1993). The most abundant subunit of native neurofilaments is NF-L, which has been suggested to form a "core" filament with which NF-M and NF-H coassemble (Delacourte et al., 1980; Geisler and Weber, 1981; Liem and Hutchison, 1982; Hisanaga and Hirokawa, 1988; Troncoso et al., 1990). Whereas NF-L self-assembles into intermediate filament (IF)-like structures in vitro, NF-M and NF-H only produce short, kinky filaments (e.g., Delacourte et al., 1980; Geisler and Weber, 1981; Liem and Hutchison, 1982; Aebi et al., 1988; Troncoso et al., 1989; Hisanaga and Hirokawa, 1988, 1989). The COOH-terminal tails of NF-M and NF-H project as "sidearms" that extend radially 55 and 63 nm, respectively, from the filament shaft (Hisanaga and Hirokawa, 1988; Troncoso et al., 1990; Gotow et al., 1992). Typical for IF structures in the electron microscope, filaments reconstituted from NF-L appear as relatively featureless 10-nm filaments after negative staining, although sometimes protofilament-like structures can also be observed (e.g., Geisler and Weber, 1981; Liem and Hutchison, 1982; Aebi et al., 1988; Troncoso et al., 1990). When glycerol-sprayed onto freshly cleaved mica and rotary metal-shadowed, the same filaments exhibit a characteristic ~21-nm axial repeat of beaded segments (e.g., Milam and Erickson, 1982; Aebi et al., 1988; Hisanaga and Hirokawa, 1988; Troncoso et al., 1990; Gotow et al., 1992).

Common to all IF polypeptides is a conserved "rod" domain (e.g., Geisler and Weber, 1982; Hanukoglu and Fuchs,

Address all correspondence to Dr. Ueli Aebi, M. E. Müller Institute at the Biocenter, University of Basel, Klingelbergstrasse 70, CH-4056 Basel, Switzerland.

1. *Abbreviations used in this paper*: FWHM, full-width-half-maximum; IF, intermediate filament; MPL, mass-per-length; NFs, neurofilaments; SFM, scanning force microscopy; STEM, scanning transmission electron microscopy; TEM, transmission electron microscopy.

1982, 1983; Steinert et al., 1983; for a review see Steinert and Roop, 1988), which due to its distinct heptad-repeat sequence pattern forms parallel, unstaggered two-stranded α-helical coiled-coils (e.g., Parry et al., 1985; Quinlan et al., 1986; Aebi et al., 1986, 1988; for a review see Parry and Steinert, 1992). In the case of NF-L, the rod domain is 308-amino acid long and is sandwiched between a 93-amino acid long NH_2-terminal head domain and a 142-amino acid long COOH-terminal tail domain (Lewis and Cowan, 1985; Geisler et al., 1985*a*). The central rod with its periodic distribution of charged residues is thought to be important for the lateral interaction of dimers to form tetramers and possibly higher-order oligomers (e.g., McLachlan and Stewart, 1982; Crewther et al., 1983; for a review see Parry and Steinert, 1992).

Although the head and tail domains flanking the α-helical rod are of variable size and character among different IF subunits (for a review see Steinert and Roop, 1988), two short sequences of positively and negatively charged residues at the COOH- and NH_2-terminal ends of the rod reveal a remarkably high conservation among the different types of IF proteins (e.g., Conway and Parry, 1988; Letai et al., 1992). Deletion and point mutations within these two short regions, coupled with transfection and in vitro assembly studies, have indicated that these two sites may play a crucial role in the association of IF dimers into distinct higher-order structures (e.g., Albers and Fuchs, 1987, 1989; Heald and McKeon, 1990; Coulombe et al., 1990; Hatzfeld and Weber, 1991; Letai et al., 1992). In fact, single-point mutations in these highly conserved rod domain sequences of human epidermal keratins appear to be the proximal cause of two skin blistering diseases (e.g., Bonifas et al., 1991; Coulombe et al., 1991; Lane et al., 1992; Rothnagel et al., 1992; Cheng et al., 1992; Chipev et al., 1992; for recent reviews see Fuchs and Coulombe, 1992; Coulombe, 1993).

Although tetramers do form with only the rod domain (e.g., Geisler et al., 1985*b*, 1992), a priori it is not evident to what extent the lateral association of two IF dimers into a tetramer is influenced by the presence of the NH_2-terminal head and/or COOH-terminal tail domains. On the one hand, electron micrographs of what were assumed to be IF tetramers have been interpreted to represent an approximately in-register alignment of the two dimers within the tetramer in either a parallel (e.g., Ip et al., 1985; Ip, 1988; Quinlan et al., 1984; Hisanaga et al., 1990; Hisanaga and Hirokawa, 1990; Coulombe and Fuchs, 1990) or an antiparallel (Geisler et al., 1985*b*; Steinert, 1991*a*) fashion. On the other hand, both EM and chemical cross-linking of tetrameric rods, protofilaments, and assembled IFs have indicated that tetramers are also formed by antiparallel, staggered association of two dimers (e.g., Ip et al., 1985; Potschka et al., 1990; Coulombe and Fuchs, 1990; Steinert, 1991*a*; Geisler et al., 1992). Possibly unifying these various findings, analysis of the mechanism of in vitro assembly of mouse and human keratins has suggested that IFs are built from multiple oligomeric units rather than a unique tetrameric building block (Coulombe and Fuchs, 1990; Steinert, 1991*b*). Extending these latter studies, chemical cross-linking has yielded three dominant modes of antiparallel assembly for keratin (Steinert and Parry, 1993; Steinert et al., 1993*a*,*b*), vimentin (Steinert et al., 1993*c*), and desmin (Geisler et al., 1992; Geisler, 1993) dimers: the first involves dimers in approximate register, while in the second dimers are staggered so as to bring the helix 1B segments into approximate alignment, and in the third dimers are staggered so as to bring the helix 2B segments into approximate register.

Whereas it remains to be seen what specific—if any—role(s) the two end domains play in IF tetramer formation, it is without question that assembly of the tetrameric building blocks into higher-order oligomers and ultimately bona fide 10-nm filaments requires at least some parts of one or both end domains to be present. For instance, it has been demonstrated that removal of at least some portions of the NH_2-terminal head domain of keratins has deleterious effects to filament formation in vivo and in vitro (e.g., Sauk et al., 1984; Albers and Fuchs, 1989; Coulombe et al., 1990; Bader et al., 1991; Wilson et al., 1992). On the other hand, at least in some (e.g., Hatzfeld and Weber, 1990; Bader et al., 1991; Wilson et al., 1992)—but not all (e.g., Kouklis et al., 1991)—cases, both the type I and type II tail domains of keratins appear to be dispensable for IF assembly. Proteolysis (Geisler et al., 1982; Kaufmann et al., 1985), mutagenesis (Raats et al., 1990, 1991; Eckelt et al., 1992; Herrmann et al., 1992; McCormick et al., 1993), and the use of antibodies or synthetic peptides (Birkenberger and Ip, 1990; Hofmann and Herrmann, 1992) have all demonstrated that head or tail domain sequences can markedly affect assembly of desmin and vimentin into IFs. For the nuclear lamins (i.e., type V IF proteins) too, in vitro studies with full length and truncated human, *Xenopus* and chicken isoforms have shown that both the NH_2- and COOH-terminal end domains are implicated in filament formation (Moir et al., 1991; Gieffers and Krohne, 1991; Heitlinger et al., 1992). Taken together, consideration of all of these reports makes it difficult to come to a consensus on the exact contributions of the head and tail domains to IF assembly. Nevertheless, in general the NH_2-terminal head domain appears to play a more important role for filament formation than the COOH-terminal tail domain.

For type IV IF proteins specifically, transfection studies with COOH- and NH_2-terminal mutants of NF-L and NF-H have already implicated both their head and tail domains in neurofilament formation (Gill et al., 1990; Wong and Cleveland, 1990; Chin et al., 1991). To investigate more systematically the influence of the NH_2-terminal head, the central rod, and the COOH-terminal tail domain on the structure and in vitro assembly properties of NF-L, full-length mouse NF-L was expressed in *E. coli*, purified, and compared with authentic NF-L isolated from bovine spinal cord. In addition, using the same bacterial expression system, recombinant headless, tailless, and rod NF-L fragments were produced, and their structure and assembly properties explored by conventional and scanning transmission electron microscopy (TEM and STEM).

Materials and Methods

(a) Construction of Bacterial Expression Plasmids for Full-length and Truncated Mouse NF-Ls

To facilitate the cloning of full-length and truncated NF-L cDNAs into the bacterial expression vector pET11a, a PCR strategy was employed whereby pairs of synthetic oligonucleotide primers were used to introduce an

Nde I site at the translation start codon (ATG) at the 5′ end, and a stop codon (TGA) followed by a *Bam HI* site at the 3′ end of each construct (see Fig. 1 *a*). The parental plasmid pMSV-NF-L cDNA representing the full-length mouse NF-L sequence (Fig. 1 *a*; see also Gill et al., 1990) was used to prime the synthesis of each of the PCR products encoding NF-L (full-length), NF-L-NΔ84 (nearly headless), NF-L-NΔ93 (exactly headless), NF-L-CΔ128 (nearly tailless), and NF-L-NΔ84/CΔ128 (rod) (Fig. 1 *b*). Each of the PCR products was digested with *Nde I* and *Bam HI*, gel purified, and ligated to the pET11a expression vector (Novagen, Inc., Madison, WI), previously digested with *Nde I-Bam HI*, to yield the expression plasmids pET11a-NF-L, pET11a-NF-L-NΔ84, pET11a-NF-L-NΔ93, pET11a-NF-L-CΔ128, and pET11a-NF-L-NΔ84/CΔ128. The terminal sequences of each construct were verified by the dideoxy-chain termination method.

(b) Bacterial Expression and Purification of Full-length and Truncated Mouse NF-Ls

Each plasmid was transformed into bacterial strain HMS 174 (Studier and Moffat, 1986), and overnight cultures were diluted 1:100 with fresh LB-medium (10 *g* Bacto-Tryptone, 5 *g* Bacto-Yeast Extract [both from Difco, Detroit, MI], and 5 *g* NaCl in 1 liter H_2O). Cells were grown to an OD_{600} of 0.8 in the presence of 50 μg/ml ampicillin before they were induced with 0.4 mM Isopropyl-β-D-thiogalactopyranoside (IPTG; Biofinex, Praroman, Switzerland). After another 2 h at 37°C, the cells were pelleted and resuspended in one tenth of the original volume in "standard filament forming" buffer (50 mM MES, 170 mM NaCl, 1 mM DTT, pH 6.25). The cells were lysed with a French press at a pressure of 20,000 p.s.i. and centrifuged at 8,000 *g* for 15 min at 4°C. In the case of the full-length polypeptide and the headless NF-L fragment, 50–70% of the recombinant protein remained in the supernatant. Incubation of these supernatants for 3 h at 37°C caused the proteins to aggregate so that they became pelletable after centrifugation at 100,000 *g* for 20 min at 25°C. The pellets containing the aggregated NF-L proteins were washed twice with standard filament forming buffer before they were dissolved in "urea" buffer (25 mM Na-phosphate, pH 7.5, 6 M urea, 1 mM EGTA, and 1 mM DTT). In the case of the tailless and rod NF-L fragments, nearly 100% of the expressed protein was pelleted after centrifugation of the disrupted cells, indicating that these recombinant constructs formed inclusion bodies. The resulting pellets were washed two times with standard filament forming buffer before they were solubilized in urea buffer. To remove insoluble material, all urea-solubilized samples were centrifuged at 10,000 *g* for 10 min at 4°C before their supernatants were loaded onto a Mono Q HR 5/5 anion exchange FPLC column. The column was eluted with a linear 0–500 mM NaCl gradient in urea buffer and 1-ml fractions were collected. The fractions enriched in full-length or headless NF-L eluted between 350 and 400 mM NaCl, whereas the fractions enriched in the tailless or rod NF-L fragment eluted between 45 and 100 mM NaCl. These fractions were pooled and either used directly or stored at −70°C for later experiments. As documented in Fig. 2, for each NF-L construct the final products were >95% pure with a yield of 5–45 mg protein per liter of bacteria.

(c) Purification of Authentic NF-L from Bovine Spinal Cord

Authentic NF-L was isolated from bovine spinal cord and purified as described previously (Troncoso et al., 1990). Briefly, the native NF polypeptide triplet was extracted from fresh or deep-frozen bovine spinal cords in 100 mM MES (2-morpholino-ethane-sulfonic acid), pH 6.5, containing 1 mM EGTA, 0.5 mM $MgCl_2$ plus protease inhibitors, as described by Delacourte et al. (1980). After two centrifugation steps, the last pellet containing the three NF polypeptides was resuspended in urea buffer (see [b] above), and chromatographed on a Sephadex G-25 column. The resulting void volume was loaded onto a Mono Q HR 5/5 anion exchange FPLC column (Pharmacia, Uppsala, Sweden) and eluted with a 0–500 mM NaCl step gradient in urea buffer. Fractions containing the different NF polypeptides were identified by SDS-PAGE.

(d) In Vitro Assembly

Assembly of full-length NF-L and the headless, tailless, and rod NF-L fragments was started from their denatured form in 6 M urea buffer. Generally, 100-μl aliquots (at a protein concentration of 0.5–1.5 mg/ml) were used for dialysis. For the reconstitution of authentic and recombinant full-length NF-L into 10-nm filaments, aliquots were dialyzed overnight at 37°C against standard filament forming buffer (50 mM MES, 170 mM NaCl, 1 mM DTT, pH 6.25), and for comparison, dialysis was performed against the same buffer but at the more physiological pH of 7.5. With the headless NF-L fragment, filaments were obtained after dialysis overnight at room temperature against 50 mM MES, 2–25 mM $CaCl_2$, 1 mM DTT, pH 6.0. The tailless NF-L fragment produced filamentous structures after dialysis for ≥3 h at room temperature against 50 mM Hepes, 1 mM $CaCl_2$, 1 mM DTT, pH 7.5. Raising the Ca^{2+}-concentration to 5–10 mM yielded paracrystalline fibers, and with Ca^{2+}-concentrations >20 mM, large, three-dimensional aggregates with paracrystalline order were obtained. Also, with the NF-L rod fragment paracrystal-like structures formed after dialyzed for ≥12 h at room temperature against 50 mM MES, 20 mM $CaCl_2$ or $MgCl_2$, 1 mM DTT, pH 6.0–7.0.

(e) SDS-PAGE and Immunoblotting

For SDS-PAGE samples were run on 10.5% polyacrylamide gels and stained with Coomassie brilliant blue R. For immunoblotting, the protein was electrophoretically transferred to a nitrocellulose sheet (BA 85, Schleicher and Schuell, Dassel, Germany) as described by Towbin et al. (1979). After transfer, the nitrocellulose was blocked for 30 min with 5% milkpowder in TBS (10 mM Tris, 150 mM NaCl, pH 7.5). As the primary antibody, we used a monoclonal anti-neurofilament 68 kD antibody (obtained from Boehringer, Mannheim, Germany). The secondary antibody was a horseradish peroxidase–conjugated rabbit anti-mouse IgG (DAKO-Immunoglobulins, Glostrup, Denmark). Antibody conjugates were visualized with 4-chloro-1-naphthol (Fluka, Buchs, Switzerland).

(f) Electron Microscopy

For negative staining, a 5-μl aliquot of the sample was adsorbed for 60 s to a glow-discharged (Aebi and Pollard, 1987) carbon-coated collodium film on a copper grid. The grid was washed with two drops of distilled water, stained for 15 s with 0.75% uranyl formate (pH 4.25), and air-dried after removal of excess liquid with filter paper followed by suction with a capillary applied to the edge of the grid.

For glycerol spraying/rotary metal shadowing, a 20-μl aliquot of the sample was mixed with glycerol to a final concentration of 30% and sprayed onto freshly cleaved mica. The mica piece was placed en face on the rotary table of a freeze-etch apparatus (Balzers BAE 080) and rotary-shadowed with platinum/carbon at an elevation angle of ~3° (Fowler and Aebi, 1983).

For thin sectioning, paracrystalline arrays and filamentous structures were prefixed with 1.5% glutaraldehyde for ~90 min at 4°C. After washing six times for 15 min each with cold dialysis buffer, the samples were fixed with 1% osmium tetroxide for 90 min at 4°C and dehydrated with 50% ethanol for 10 min at 4°C, followed by 70% ethanol for 20 min at room temperature. Postfixation was with 2% uranyl acetate in 70% ethanol for 1 h at room temperature. The samples were further dehydrated with 90% ethanol for 30 min, washed twice for 60 min at room temperature with 100% ethanol, and finally washed for 10 min in pure propylenoxide. Next the samples were infiltrated with a graded series of Epon 812:propylenoxide mixtures (1:2 for 1 h, 1:1 for 1 h, and 2:1 overnight). The next day the samples were embedded in pure Epon resin using gelatin capsules and cured first at 45°C for 24 h, and then at 60°C for 72 h. After thin sectioning using an Ultracut (Reichert-Jung Optische Werke, Vienna, Austria) microtome, sections were poststained for 35 min with 6% uranyl acetate followed by incubation for 45 s with lead acetate (Millonig, 1961).

Specimens were examined in a Hitachi H-7000 (Hitachi, Ltd., Tokyo, Japan) TEM operated at either 100 kV (for negatively stained and metal shadowed specimens) or 75 kV (for embedded/thin-sectioned material). Electron micrographs were recorded on Kodak SO-163 (Eastman Kodak Comp., Rochester, NY) electron image film at nominal magnifications of either 20,000 ×, 30,000 ×, or 50,000 ×. Magnification calibration was performed according to Wrighley (1968) using negatively stained catalase crystals.

The full-width-half-maximum (FWHM) and mass-per-length (MPL) of unstained/freeze- or air-dried NF-L filaments were determined by quantitative STEM, using a Vacuum Generators (East Grinstead, Great Britain) HB-5 STEM operated at 80 kV, exactly as described by Engel et al. (1985). To avoid partial unraveling of the filaments on the EM grid they were fixed with 0.1% glutaraldehyde at room temperature for 10 min. Adsorption of these samples to glow-discharged thin carbon films was followed by four washes with quartz-distilled water.

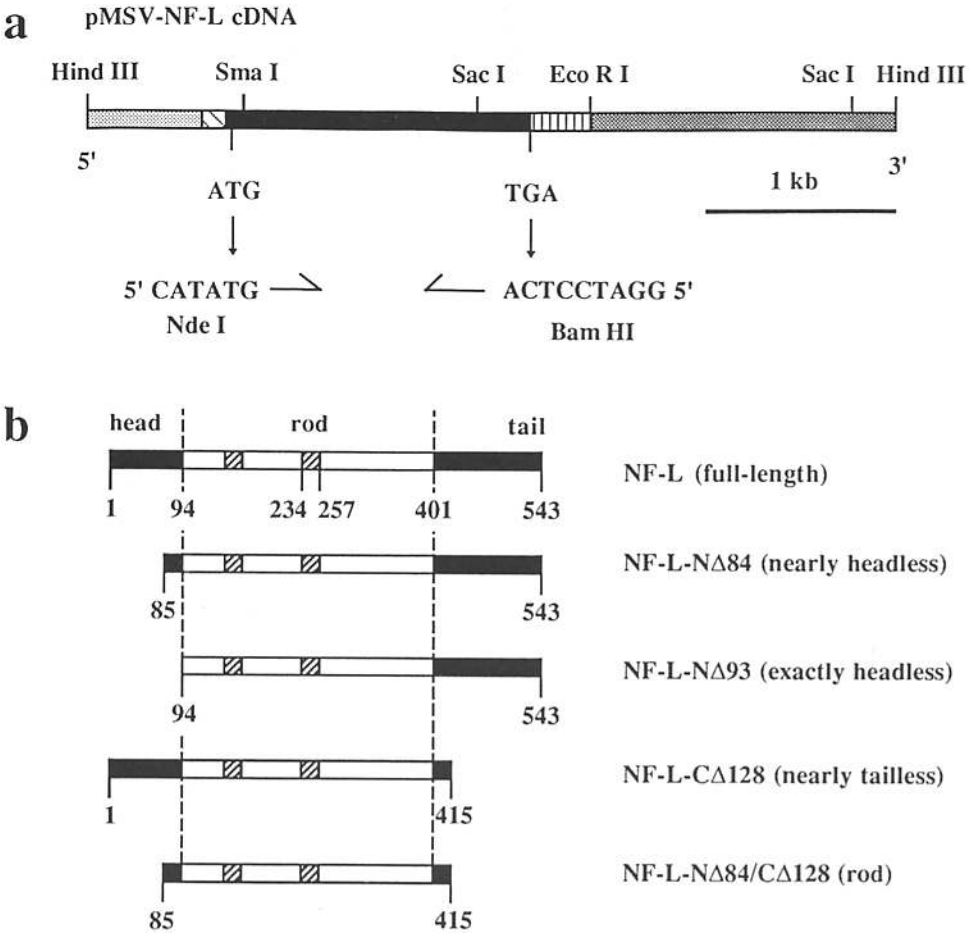

Figure 1. NF-L cDNA constructs used to express various NF-L fragments in *E. coli*. All constructs were generated by PCR, whereby pairs of synthetic oligonucleotide primers were used to introduce an Nde I site at the translation initiation codon (*ATG*) at the 5′ end, and a stop codon (*TGA*) followed by a Bam HI site at the 3′ end of each construct. (*a*) Parental plasmid pMSV-NF-L cDNA representing the full-length mouse NF-L sequence, with ▨, MSV promoter; ▧, NF-L 5′ untranslated region; ■, mouse NF-L cDNA; ▥, NF-L 3′ untranslated region; ■, 3′ flanking region. (*b*) Schematic drawings of the full-length and various truncated NF-L polypeptides encoded by a series of pET-NF-L cDNA constructs. ■, head or tail domain; ▭, α-helical regions of the rod domain; ▨, helix linker regions.

Results

To assess the roles of the 93-amino acid long NH_2-terminal head, 308-amino acid long rod and 142-amino acid long COOH-terminal tail domains in NF-L assembly, a full-length, two 'headless' (NF-L-NΔ84 and NF-L-NΔ93), a 'tailless' (NF-L-CΔ128), and a rod (NF-L-NΔ84/CΔ128) construct were engineered from a mouse NF-L cDNA (see Fig. 1 *a*; Lewis and Cowan, 1985). As described in Materials and Methods, each construct was expressed in bacteria and the recombinant protein purified to better than 95% (see Fig. 2).

(a) Structure and Assembly Properties of Recombinant full-length Mouse NF-L, and Comparison with Authentic Bovine NF-L

As illustrated in Figs. 3 and 4, when dialyzed overnight into standard filament forming buffer (i.e., 50 mM MES, 170 mM NaCl, 1 mM DTT, pH 6.25), recombinant full-length mouse NF-L (Fig. 4) exhibited assembly properties that were very similar to those of authentic NF-L isolated from bovine spinal cord (Fig. 3). In negatively stained preparations both authentic (Fig. 3 *a*) and recombinant (Fig. 4 *a*) NF-L yielded a mixture of "compact" and "partially unraveled" filaments with lengths ranging from 0.5 to several μm. While the more abundant compact, featureless filaments revealed an apparent diameter typical for IFs (i.e., ~10 nm; see Table I), the partially unraveled filaments unveiled the subfilamentous IF organization (c.f., Franke et al., 1982; Aebi et al., 1983, 1988; Troncoso et al., 1990). As documented in Table I, when prepared by glycerol spraying/rotary metal shadowing both authentic (Fig. 3 *b*) and recombinant (Fig. 4 *b*) NF-L filaments revealed a 21-nm axial "beading" diagnostic for IFs (Milam and Erickson, 1982; Henderson et al., 1982; Aebi et al., 1983, 1988; Hisanaga and Hirokawa, 1988; Troncoso et al., 1989, 1990; Gotow et al., 1992). Raising the pH of the standard filament forming buffer from its optimal value of 6.25 to the more physiological value of 7.5 produced only short (≤100 nm), less than 10-nm wide kinky filamentous assemblies after dialysis of urea-solubilized authentic (Fig. 3 *c*) or recombinant (Fig. 4 *c*) NF-L against otherwise standard filament forming buffer. These short filamentous assemblies appeared rather unstable in the sense that they frequently splayed or unraveled into distinct subfilamentous structures.

Taken together, under standard filament forming conditions the 10-nm filaments assembled from recombinant mouse NF-L appeared indistinguishable from those made of authentic bovine NF-L both by negative staining and glycerol spraying/rotary metal shadowing. Compared to bona fide type I/II or type III IFs, both authentic and recombinant NF-L 10-nm filaments are relatively short and irregular with a clear tendency to partially unravel. The reason for these differences is unclear but may be related to the fact that in vivo neurofilaments are obligate heteropolymers (Lee et al., 1993; Ching and Liem, 1993).

To assess more quantitatively the possible differences be-

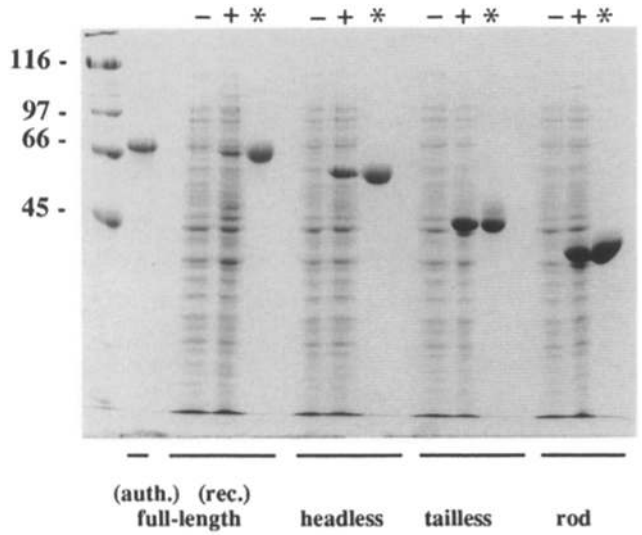

Figure 2. Purified authentic bovine NF-L, and the expression and purification of bacterially expressed full-length mouse NF-L, and the mouse NF-L fragments headless, tailless, and rod monitored by SDS-PAGE (10.5%; stained with Coomassie blue). Uninduced (−) and induced (+) bacteria after transformation with the respective expression plasmids (the equivalent of 150 μl of bacterial culture was loaded onto each lane), and (*) purified NF-L or NF-L fragments. (Lane *1*) Purified authentic NF-L isolated from bovine spinal cord; (lanes *2–4*) bacterially expressed full-length mouse NF-L; (lanes *5–7*) bacterially expressed headless mouse NF-L; (lanes *8–10*) bacterially expressed tailless mouse NF-L; and (lanes *11–13*) bacterially expressed mouse NF-L rod domain. Gel standards with their respective *MW*, β-galactosidase, 116 kD; *phosphorylase b*, 97 kD; *bovine albumin*, 66 kD; and *ovalbumin*, 43 kD.

tween recombinant and authentic NF-L filaments produced under standard filament forming conditions, we measured their FWHM and MPL by STEM of lightly fixed (with 0.1% glutaraldehyde), unstained specimens (Figs. 3 *d* and 4 *d*; see Materials and Methods). As listed in Table I, the standard filaments made of authentic NF-L (Fig. 3, *d* and *e*) yielded an average FWHM of 9.2 ± 1.0 nm and an average MPL of 47 ± 7 kD/nm compared to an average FWHM of 10.1 ± 0.8 nm and an average MPL of 57 ± 6 kD/nm for the standard filaments assembled from recombinant NF-L (Fig. 4, *d* and *e*). These MPL values amount to ~33 polypeptides per filament cross-section for the authentic NF-L filaments, and ~41 polypeptides per filament cross-section for the recombinant NF-L filaments, thus yielding a statistically significant difference of ~10 kD/nm, or roughly eight polypeptides per filament cross-section.

The reason for this significant MPL difference between authentic and recombinant NF-L filaments assembled under identical conditions is unclear. As we are comparing authentic bovine NF-L with recombinant mouse NF-L, it is conceivable that this difference is primarily species-specific. Other, possibly more important differences may be due to posttranslational modifications such as phosphorylation or glycosylation by which authentic NF-L may be distinct from bacterially expressed NF-L (see Discussion).

(b) Structure and Assembly Properties of Headless Mouse NF-L

To determine the role of the NH_2-teminal head domain of NF-L in IF assembly, in vitro reconstitution experiments were performed with NF-L-NΔ84, a truncated mouse NF-L protein missing all but the last nine amino acid residues of its NH_2-terminal head domain. As illustrated in Fig. 5 *a*, dialysis of this nearly headless NF-L protein into standard filament forming buffer produced 30–50 nm long rod-like particles with a definite tendency to associate longitudinally when viewed by glycerol spraying/rotary metal shadowing. Most likely, these rod-like particles represent tetramers made of two dimers interacting laterally in an antiparallel fashion with a 20–30 nm overlap, i.e., approximately half-staggered (see Fig. 8 *a* and Discussion). In contrast to tailless NF-L and NF-L rod (see [*c*] and [*d*] below), the protofilaments made of headless NF-L did not exhibit any significant tendency to further aggregate laterally in standard filament forming buffer. For lateral aggregation of the protofilaments to ensue, ≥2 mM $CaCl_2$ or $MgCl_2$ had to be added to standard filament forming buffer (data not shown). Ca^{2+}- or Mg^{2+}-dependent lateral aggregation of protofilaments became even more effective when at the same time the ionic strength (i.e., the NaCl concentration) was lowered.

As documented in Fig. 5, *b* and *c*, the headless NF-L construct formed long filamentous structures after overnight dialysis at room temperature of urea-solubilized material into pH 6 MES buffer containing 2–25 mM $CaCl_2$ (see Materials and Methods). These headless NF-L filaments were significantly longer (several μm) and thinner (8.3 ± 0.8 nm; see Table I) than the ~10-nm diameter filaments produced from full-length authentic or recombinant NF-L (compare Fig. 5 *b* with Figs. 3 *a* and 4 *a*). After glycerol spraying/rotary metal shadowing (Fig. 5 *c*), the headless NF-L filaments yielded partially unraveled bundles of protofilaments (compare with Fig. 5 *a*) that apparently lacked the 21-nm axial beading diagnostic for bona fide IFs (see Figs. 3 *b* and 4 *b*) except in places with strong unraveling (see Fig. 5 *c*; *arrowheads*). In agreement with this finding, when imaged with a scanning force microscope (SFM) in their native buffer environment, headless NF-L filaments adsorbed to glass surfaces also tended to unravel into protofilaments (data not shown). This and the reduced amount of filaments on the EM grid after glycerol spraying/rotary metal shadowing indicated that the lateral interaction of the protofilaments within the headless NF-L filaments was significantly weaker than in the 10-nm filaments produced from full-length NF-L. Interestingly, unlike the 10-nm filaments assembled from full-length NF-L which always yielded some partially unraveled filaments when negatively stained with uranyl acetate or formate (pH 4.0–4.5; see Figs. 3 *a* and 4 *a*), or when imaged by SFM in their native buffer environment (data not shown), headless NF-L filaments did not exhibit any significant unraveling after negative staining with uranyl formate or acetate (Fig. 5 *b*), indicating that these salts stabilized the lateral interaction of the protofilaments within the headless NF-L filaments. In contrast, negative staining of the same headless NF-L filaments with Na-phosphotungstate (pH 7.0) caused complete dissociation of the filaments into protofilaments and small oligomers (data not shown).

To exclude the possibility that filament formation of the

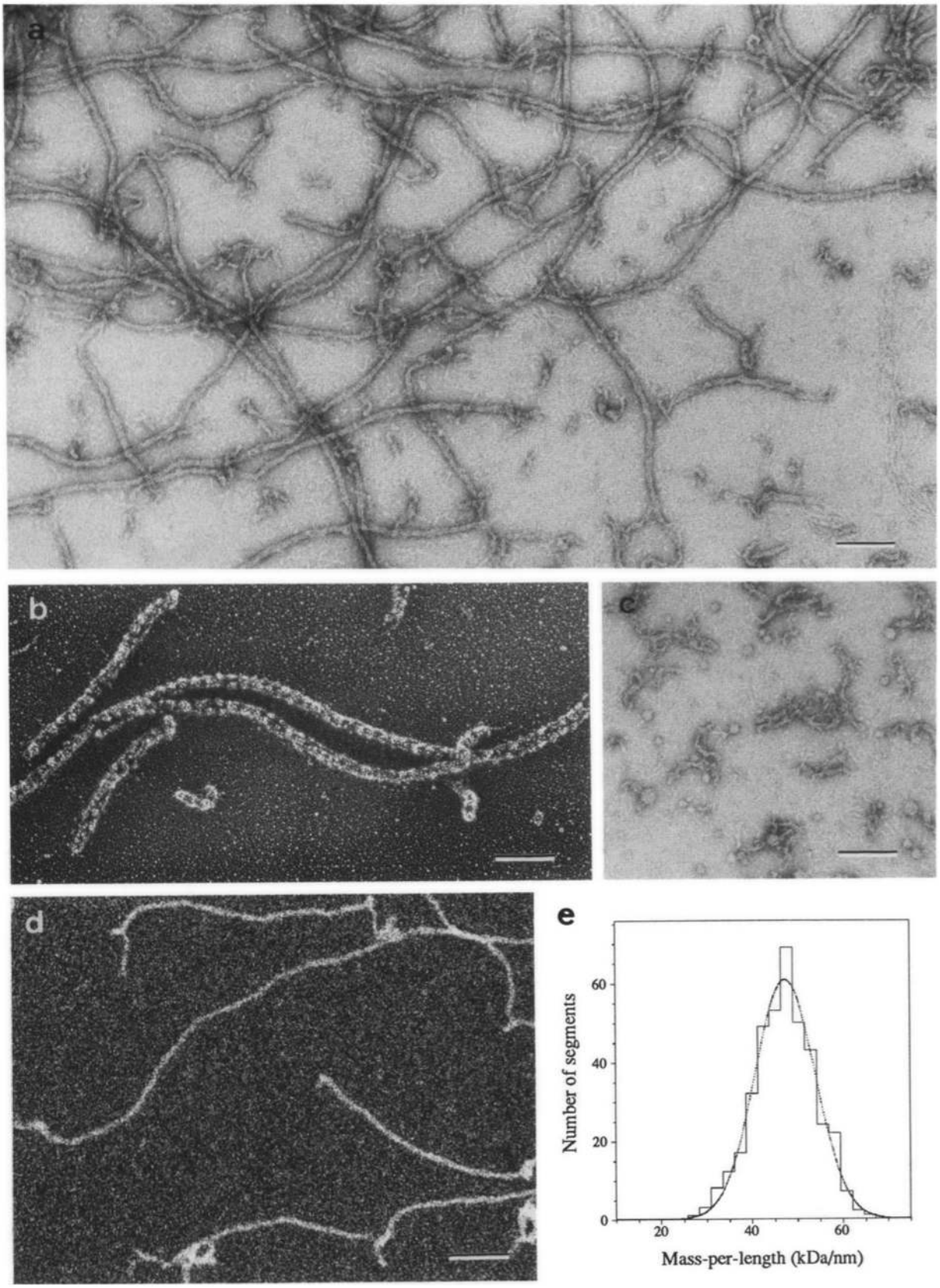

Figure 3. Assembly properties of authentic NF-L isolated from bovine spinal cord. (*a*, *b*, and *d*) Filaments obtained after dialysis of urea-solubilized material against 50 mM MES, 170 mM NaCl, 1 mM DTT, pH 6.25 (standard filament forming buffer) for ≥12 h at 37°C, or (*c*) short, kinky filamentous structures formed after dialysis against 50 mM Hepes, 170 mM NaCl, 1 mM DTT, pH 7.5 ("near-physiological" buffer) for ≥12 h at room temperature. In *a* and *c* the samples were negatively stained, in *b* the material was glycerol-sprayed/rotary metal-shadowed, and in *d* the filaments were fixed with 0.1% glutaraldehyde and freeze-dried unstained for observation in the STEM. STEM MPL data were obtained from 512 × 512-pixel frame low-dose images recorded with a pixel size of 0.9 nm and an average electron dose of 370 ± 44 e^-/nm^2. (*e*) The MPL values of 393 individual filament stretches were pooled into a histogram which was fitted with a single Gaussian curve to yield an average MPL of 47 ± 7 kD/nm. Bars, 100 nm (*a–d*).

"nearly" headless NF-L construct was dependent on the remaining nine amino acid residues of the head domain, an "exact" headless mouse NF-L construct (NF-L-NΔ93) was engineered (see Fig. 1 *b*), expressed and purified. Upon dialysis into pH 6.0 MES buffer containing 2–25 mM $CaCl_2$, long, 8.3-nm wide filaments were obtained (data not shown) that were indistinguishable from those formed from the nearly headless NF-L-NΔ84 construct (Fig. 5 *b*).

To quantify the difference between full-length and headless NF-L filaments, we measured their FWHM and MPL by STEM of lightly fixed (with 0.1% glutaraldehyde), unstained specimens (Figs. 3 *d* and 5 *d*; see Materials and Methods). As listed in Table I, the headless NF-L filaments (Fig. 5, *d* and *e*) yielded an average FWHM of 8.5 ± 1.3 nm and an average MPL of 27 ± 7 kD/nm compared to an average FWHM of 10.1 ± 0.8 nm and an average MPL of 57 ± 6 kD/nm for the recombinant full-length NF-L filaments (Fig. 4, *d* and *e*). This dramatic MPL difference cannot simply be explained on the basis of the reduced mass of the headless NF-L fragment, which is ~55 kD compared to ~65 kD for the full-length NF-L protein, and would thus yield a MPL of ~48 kD/nm assuming the same molecular architecture as for the full-length recombinant NF-L filaments, i.e., ~41 polypeptides per filament cross-section (see [a] above).

Attempts to produce paracrystalline arrays with the headless NF-L fragment were unsuccessful. Whereas filaments with a relatively constant width (e.g., Fig. 5 *b*) were produced between pH 6 and 7 in the presence of 2–25 mM $CaCl_2$ or $MgCl_2$, above pH 7 only short, unstable filamentous particles formed, which upon addition of increasing amounts of divalent cations formed large aggregates (data not shown).

(c) Structure and Assembly Properties of Tailless Mouse NF-L

Under standard filament forming conditions the nearly tailless NF-L, recombinant NF-L-CΔ128, yielded only small amounts of rod-like particles on EM grids both by negative staining as well as after glycerol spraying/rotary metal shadowing (data not shown). Judged from the turbidity of the assembled material, it consisted of large structures—possibly aggregates of 10-nm filaments—that only poorly adsorbed to EM grids. In contrast, in the presence of mM amounts of $CaCl_2$, the tailless NF-L polypeptide assembled into filamentous and paracrystal-like structures in the pH range 6–7.5 after dialysis for ≥3 h into NaCl-free buffer at room temperature. As illustrated in Fig. 6, *a* and *b*, with 1 mM Ca^{2+} tailless NF-L formed long filaments which at pH 7.5 exhibited a strong tendency to associate laterally into filament bundles. Like the headless filaments, the tailless NF-L filaments revealed a molecular architecture distinct from that of the typical 10-nm filaments formed with full-length NF-L: (*a*) they yielded a larger apparent width in negatively stained preparations, i.e., 11.3 nm vs 10.4 nm (see Table I), and (*b*) they did not exhibit the 21-nm axial beading characteristic for bona fide IFs after glycerol spraying/rotary metal shadowing (compare Fig. 6 *b* with Figs. 3 *b* and 4 *b*). As a significant amount of the assembled material was too big to adsorb to EM grids, it was plastic-embedded and thin-sectioned (see Materials and Methods) for visualization. As documented in Fig. 6 *c*, just as the smaller structures captured in negatively stained (Fig. 6 *a*) or glycerol-sprayed/rotary metal shadowed (Fig. 6 *b*) preparations, the large assembly products consisted of bundles of tightly packed filaments.

Raising the Ca^{2+}-concentration from 1 to 10 mM at pH 7.5 led to a significant increase of the filament width. As illustrated in Fig. 6 *d*, this condition produced paracrystalline fibers exhibiting a distinct light-dark transverse banding pattern with an approximate axial periodicity of 20.8 ± 1.1 nm (see Table I). Under these conditions too, a significant amount of large aggregates formed that, when embedded and thin-sectioned, revealed similar paracrystalline structures (Fig. 6 *e*) with an approximate axial periodicity of 20.4 ± 0.9 nm (see Table I) as were obtained after negative staining (Fig. 6 *d*). As documented in Fig. 6 *f*, raising the $CaCl_2$-concentration to 20 mM induced formation of large, three-dimensional paracrystalline arrays with the same light-dark transverse banding pattern and an approximate axial periodicity of 21.2 ± 0.6 nm (see Table I). Substitution of Mg^{2+} for Ca^{2+} led to similar three-dimensional paracrystalline arrays with an approximate axial periodicity of 21 nm. Whereas all the paracrystalline arrays obtained with tailless NF-L (Fig. 6, *d–f*) yielded a light-dark transverse banding pattern with a fairly regular axial periodicity of ~21 nm (see Table I), their true axial repeat was probably more like 42 nm (see Fig. 9 *b* and Discussion).

(d) Structure and Assembly Properties of the Mouse NF-L Rod Domain

Unlike the full-length (Fig. 4, *a* and *b*), headless (Fig. 5, *b* and *c*), and tailless (Fig. 6, *a* and *b*) mouse NF-L constructs, the recombinant mouse NF-L rod domain failed to form filamentous structures under all conditions examined. Just like the tailless NF-L fragment (see [*c*] above), under standard filament forming conditions the NF-L rod domain produced large aggregates that did not stick to EM grids. While these aggregates may actually consist predominantly of small, distinct oligomers (e.g., tetramers or octamers), this behavior is very different from that of desmin and vimentin rods and the rods made of keratin pairs which form soluble tetramers under typical filament forming conditions (e.g., Sauk et al., 1984; Geisler et al., 1992). So it could be argued that this atypical behavior of the NF-L rod at pH 6.25 may simply represent "isoelectric precipitation". Arguing against this interpretation, formation of similar aggregates that also failed to adsorb to EM grids was observed after dialysis of the NF-L rod against near-physiological buffer (i.e., 50 mM Hepes, 170 mM NaCl, 1 mM DTT, pH 7.5; data not shown). Another possibility for this unusual behavior of the NF-L-NΔ84/CΔ128 rod used in this investigation may be its lack of a several residue long consensus sequence found in all IF proteins (e.g., Steinert and Roop, 1988; Steinert and Parry, 1993) which was still present in, e.g., the proteolytically produced desmin rod forming soluble tetramers at physiological salt and pH conditions (e.g., Geisler et al., 1992).

In the presence of ≥20 mM divalent cations (i.e., $CaCl_2$ or MgC_2), the NF-L rod assembled into large, precipitating aggregates after dialysis into pH 7.0 MES buffer. As documented in Fig. 7 *a*, the smaller aggregates that adsorbed to EM grids appeared as highly branched supramolecular assemblies in negatively stained preparations. Closer inspec-

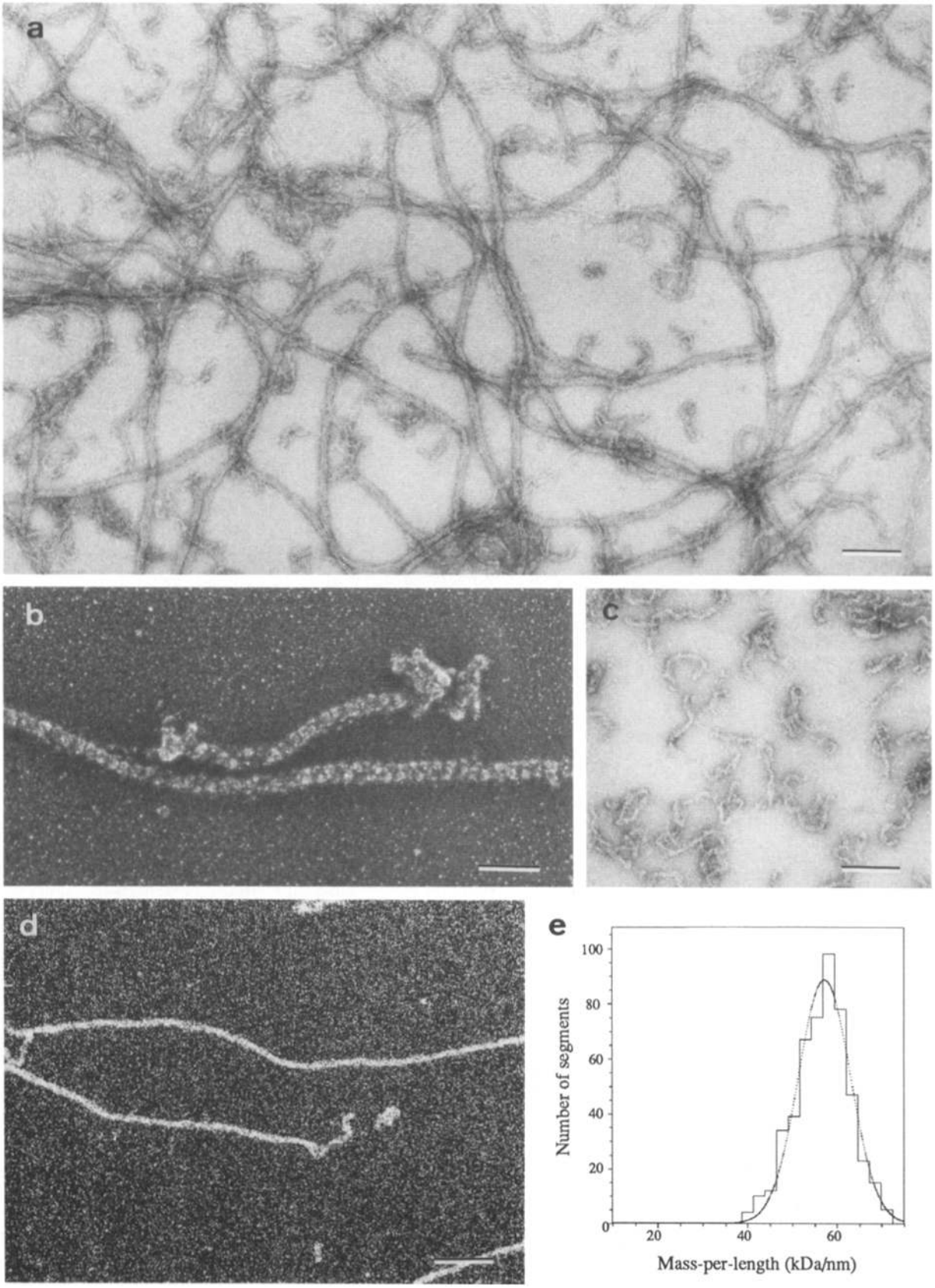

Figure 4. Assembly properties of recombinant mouse NF-L. (*a*, *b*, and *d*) Filaments obtained after dialysis of bacterially expressed, urea-solubilized mouse NF-L against 50 mM MES, 170 mM NaCl, 1 mM DTT, pH 6.25 (standard filament forming buffer) for ≥12 h at 37°C, or (*c*) short, kinky filamentous structures formed after dialysis against 50 mM Hepes, 170 mM NaCl, 1 mM DTT, pH 7.5 ("near-physiological" buffer) for ≥12 h at room temperature. In *a* and *c* the samples were negatively stained, in *b* the material was glycerol-

Table I. Various Measurements of Distinct Assembly Products of Full-length Authentic and Recombinant NL-L, and of Recombinant Headless, Tailless, and Rod Fragments of NF-L

NF-L construct	Width of filaments (*nm*)	Mass-per-length (MPL) of filaments (*kD/nm*)	Approximate axial periodicity (*nm*)
full-length NL-L (authentic)	10.2 ± 0.8 (n = 100)*		21.2 ± 0.6 (n = 390)‡
	9.2 ± 1.0 (n = 115)‖	47 ± 7 (n = 393)‖	
full-length NL-L (recombinant)	10.4 ± 1.0 (n = 100)*		21.3 ± 0.4 (n = 449)‡
	10.1 ± 0.8 (n = 293)‖	57 ± 6 (n = 507)‖	
headless NF-L	8.4 ± 0.8 (n = 100)*		–
	8.5 ± 1.3 (n = 277)‖	27 ± 7 (n = 277)‖	
tailless NF-L			–
+1 mM $CaCl_2$	11.3 ± 1.7 (n = 100)*	not measured	20.8 ± 1.1*
+10 mM $CaCl_2$	no filaments	–	20.4 ± 0.9§
+20 mM $CaCl_2$	no filaments	–	21.2 ± 0.6*
NF-L rod	no filaments	–	21.4 ± 1.4*
			20.7 ± 1.6§

The mean ± SD have been calculated for each set of n measurements.
* Negatively stained (compact filaments only were measured)
‡ Glycerol-sprayed/rotary metal-shadowed
§ Embedded/thin-sectioned
‖ Unstained (fixed with 0.1% glutaraldehyde) filaments recorded in a STEM; in the case of the filament width, the FWHM was determined (for the method see Engel et al., 1985).

tion of the thin edges of these assemblies revealed faint, light-dark transverse banding patterns (Fig. 7 *a*; *arrowheads*) with an approximate axial periodicity of 21.4 ± 1.4 nm (see Table I), indicating that they were paracrystalline in nature. Similar to the tailless NF-L fragment (see Fig. 6 *a*), when embedded and thin-sectioned, the aggregates and precipitates produced by the NF-L rod domain under these assembly conditions were made of paracrystalline fibers or "needles" exhibiting a distinct light-dark transverse banding pattern with an approximate axial periodicity of 20.7 ± 1.6 nm (see Table I). However, unlike the tailless NF-L fragment, negative stain electron microscopy of the NF-L rod domain revealed no filamentous structures or fibers at any Ca^{2+}- or Mg^{2+}-concentration tried. On the other hand, the conditions under which tailless NF-L and the NF-L rod formed paracrystalline arrays were very similar (see [*c*] above).

(e) The Origin of the 21-nm Axial Beading Observed with NF-L Filaments

To shed more light on the origin of the 21-nm axial beading commonly observed with IFs when glycerol-sprayed onto freshly cleaved mica and rotary metal-shadowed (e.g., Milam and Erickson, 1982; Henderson et al., 1982; Aebi et al., 1983, 1988; Hisanaga and Hirokawa, 1988; Troncoso et al., 1989, 1990; Gotow et al., 1992), we inspected distinct NF-L assembly intermediates and unraveling NF-L filaments by this preparation technique using both authentic and recombinant NF-L. As documented in Fig. 8 *a*, dialysis of urea-solubilized NF-L into 5 mM Pipes, 0.1 mM EGTA, 0.1 mM EDTA, 0.1 mMDTT, pH 6.8 (PEE buffer) at 4°C overnight (Hisanaga et al., 1990) yielded small oligomeric particles consisting of 3–5 beaded segments with an average axial repeat of 21 nm (see *arrowheads*). Most likely, these particles represent octamers (Hisanaga et al., 1990), i.e., pairs of approximately half-staggered tetramers. Based on these data it is difficult to decide whether the tetramers themselves have a stagger or not (e.g., Aebi et al., 1988; Coulombe and Fuchs, 1990; Steinert, 1991*b*). Similarly, as illustrated in Fig. 8 *b*, unraveling NF-L filaments (i.e., in the presence of 10 mM phosphate; e.g., Aebi et al., 1983, 1988; Troncoso et al., 1990) unveiled subfilaments also built from beaded segments with an average axial repeat of 21 nm. Probably, these subfilaments are primarily octameric protofibrils (Aebi et al., 1983) with the more massive ones being pairs of protofibrils. Occasionally, rather tenuous subfilaments can be depicted (see *arrowheads*) which most likely represent tetrameric protofilaments. Interestingly, in several instances the 21-nm beading repeat along these protofilaments or protofibrils appears irregular, alternating between shorter and longer repeats (see also Sauk et al., 1984; for a possible explanation see Fig. 9 *b* and Discussion). For comparison, Fig. 8 *c* reveals a stretch of intact NF-L filament which in places appears split into two "half-filaments" (see *arrow*) probably consisting of pairs of protofibrils (see Fig. 9 *b* and Discussion).

From these images it is evident that the appearance of beaded segments with an average, 21-nm axial repeat does not require an entire 10-nm filament. In fact, as documented in Fig. 8 *b* (*arrowheads*) and shown previously with keratins (Sauk et al., 1984; Coulombe and Fuchs, 1990), it is already

sprayed/rotary metal-shadowed, and in *d* the filaments were fixed with 0.1% glutaraldehyde and freeze-dried unstained for observation in the STEM. STEM MPL data were obtained from 512 × 512-pixel frame low-dose images recorded with a pixel size of 0.9 nm and with an average electron dose of 371 ± 47 e^-/nm^2. (*e*) The MPL values of 507 individual filament stretches were pooled into a histogram which was fitted with a single Gaussian curve to yield an average MPL of 57 ± 6 kD/nm. Bars, 100 nm (*a–d*).

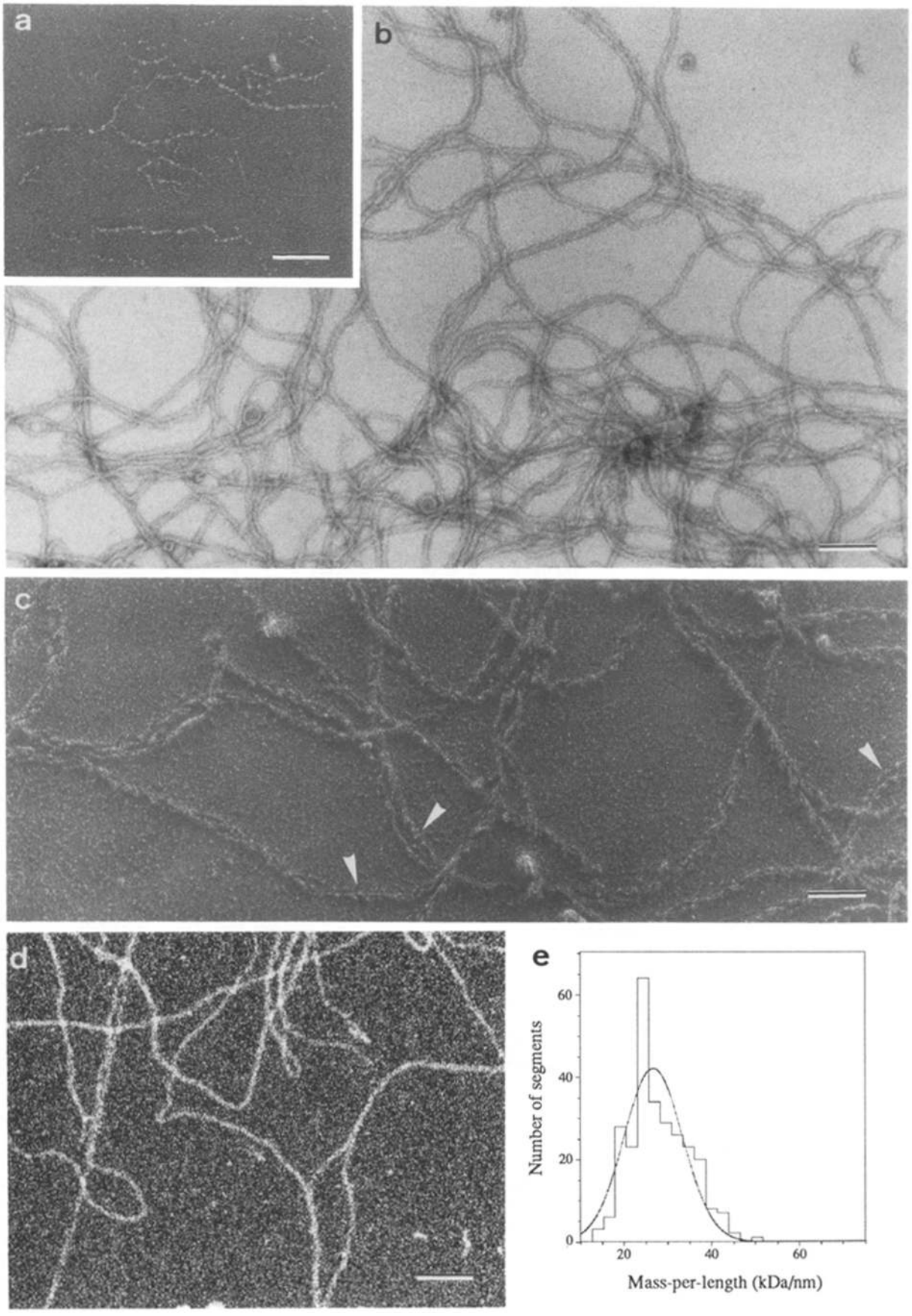
a
b
c
d
e
60
40
20
0
Number of segments
20
40
60
Mass-per-length (kDa/nm)

observed with individual tetrameric protofilaments, albeit with smaller beads and less regular repeats. Most likely, a significant contribution to the appearance of beads is made by the NH_2- and COOH-terminal end domains, as their removal attenuates or abolishes the beading (see Figs. 5 *c* and 6 *b*). An additional contribution must involve the longitudinal, head-to-tail interaction of dimers with a 1–3-nm N-C type overlap thus producing "bumps" (see Fig. 9 and Discussion). Finally, the average 21-nm axial periodicity of the beaded segments is due to an approximate half-stagger between laterally associating dimers, tetramers, or octamers (for details see Fig. 9 and Discussion).

Discussion

(a) Toward a Molecular Model for IF Architecture

How can EM and chemical cross-linking data be combined to yield a molecular model for IF architecture? The elementary building block of all IFs is the dimer formed by a parallel, unstaggered two-stranded α-helical coiled-coil with a molecular length ranging between 44 and 46 nm (e.g., Geisler et al., 1982; Hanukoglu and Fuchs, 1982, 1983; Steinert et al., 1983; Parry et al., 1985; Quinlan et al., 1986; Aebi et al., 1986, 1988; Steinert et al., 1993*a*,*c*). As illustrated in Fig. 9 *a*, at their first level of structural organization dimers interact laterally, either unstaggered or approximately half-staggered, to form tetramers (e.g., Sauk et al., 1984; Ip et al., 1985; Geisler et al., 1985*b*, 1992; Coulombe and Fuchs, 1990; Steinert, 1991*b*; Steinert et al., 1993*a*,*c*). In contrast, the nuclear lamins with a ~45-kD central rod domain (e.g., McKeon et al., 1986; Fisher et al., 1986) amounting to a dimer length *l* of 50–52 nm (e.g., Aebi et al., 1986; Moir et al., 1991; Heitlinger et al., 1991, 1992), have revealed a longitudinal, head-to-tail interaction of dimers with a 1–3-nm N-C type overlap (see Fig. 9 *a*; and Gieffers and Krohne, 1991; Heitlinger et al., 1991, 1992).

More specifically, with regard to molecular models for NF-L filament architecture, the approximate, 21-nm axial repeat of beaded segments (see Table I) observed with filaments of both authentic (Fig. 3 *b*) and recombinant (Fig. 4 *b*) NF-L after glycerol spraying/rotary metal shadowing, and the approximate, 21-nm axial periodicity (see Table I) seen in paracrystals made of tailless NF-L (Fig. 6, *d–f*) and NF-L rod (Fig. 7) impose two constraints: (*a*) As the true axial repeat *r* of either filaments or paracrystals is 42–43 nm (i.e., 2× 21–21.5 nm; see Table I) and hence shorter than the molecular length *l* of the dimer building blocks (see Fig. 9 *a*), which for NF-L is likely to be somewhere between 44 and 45 nm (e.g., Steinert et al., 1993*a*,*c*; Parry, D. A. D., personal communication), their longitudinal association must involve a 1–3-nm head-to-tail "overlap." (*b*) The approximate, 21-nm axial periodicity found in both filaments and paracrystals must involve an approximate "half-stagger" between at least some of the dimers when they associate laterally to form higher-order oligomers.

In Fig. 9 *b* an attempt has been made to use these two constraints to design packing models for protofilaments, protofibrils, and half-filaments, and to deduce the "periodicity patterns" they produce, i.e., as manifested by the axial beading observed with filaments, or the transverse banding patterns seen with paracrystalline arrays. It should be stressed, however, that the hierarchy of the three types of lateral dimer–dimer interactions (Fig. 9 *a*) involved—the occurrence of all of which has been documented by chemical cross-linking (e.g., Geisler et al., 1992; Geisler, 1993; Steinert et al., 1993*a*,*b*,*c*)—is ambiguous. In these packing models, the approximate, 21-nm axial periodicity represents the average of the two axial periodicities r_1 and r_2, which are determined by the exact stagger *s* respectively overlap *o* between dimers (see Fig. 9 *a*), with $r_1 + r_2 = r$ being the true axial repeat (see Fig. 9 *b*). What implications does the proposed NF-L dimer packing model which, conceptually, is very similar to the IF model proposed recently based on keratin and vimentin cross-linking data (Steinert et al., 1993*a*,*c*) have for IF structure and assembly in general?

In both models the longitudinal association of dimers involves a short head-to-tail overlap (see Fig. 9 *a*): in our model it is somewhere between 1 and 3 nm (see above), whereas in the Steinert and Parry model it is 1.01 nm for keratin (i.e., with a molecular length of 46.22 nm) and 1.2 nm for vimentin (i.e., with a molecular length of 43.91 nm) IFs (Steinert et al., 1993*c*). This overlap may explain the remarkably high conservation of short sequences of positively and negatively charged residues found among different types of IF proteins (e.g., Conway and Parry, 1988; Letai et al., 1992). Hence, it is not surprising that deletions and point mutations within these two short end segments have profound effects on the association of IF dimers into distinct higher-order structures (e.g., Albers and Fuchs, 1987, 1989; Gill et al., 1990; Wong and Cleveland, 1990; Coulombe et al., 1990; Hatzfeld and Weber, 1991; Letai et al., 1992), and in several cases appear to be the proximal cause of genetic skin diseases of keratin (for review see Fuchs and Coulombe, 1992; Coulombe, 1993).

As suggested by the packing models in Fig. 9 *b* and documented with NF-L data in Fig. 8 (see also Sauk et al., 1984; Ip et al., 1985; Coulombe and Fuchs, 1990), contrary to the "surface lattice" model (e.g., Steinert et al., 1993*a*), observation of the approximate, 21-nm axial periodicity does

Figure 5. Assembly properties of bacterially expressed headless mouse NF-L. (*a*) Protofilamentous structures produced after dialysis of urea-solubilized headless mouse NF-L against 50 mM MES, 170 mM NaCl, 1 mM DTT, pH 6.25 (standard filament forming buffer) for ≥12 h at 37°C. Short protofilaments together with protofilamentous particles predominate. (*b–d*) Filaments obtained after dialysis of urea-solubilized headless mouse NF-L against 50 mM MES, 1 mM DTT, pH 6.0, containing 6 mM $CaCl_2$ for ≥12 h at room temperature. In *a* and *c* the samples were glycerol-sprayed/rotary metal-shadowed (*arrowheads* in *c* point to ~21-nm axial beading repeats), in *b* the material was negatively stained, and in *d* the filaments were fixed with 0.1% glutaraldehyde and freeze-dried unstained for observation in the STEM. STEM MPL data were obtained from 512 × 512-pixel frame low-dose images recorded with a pixel size of 0.9 nm and with an average electron dose of 318 ± 32 e^-/nm^2. (*e*) The MPL values of 277 individual filament stretches were pooled into a histogram which was fitted with a single Gaussian curve to yield an average MPL of 27 ± 7 kD/nm. Bars, 100 nm (*a–d*).

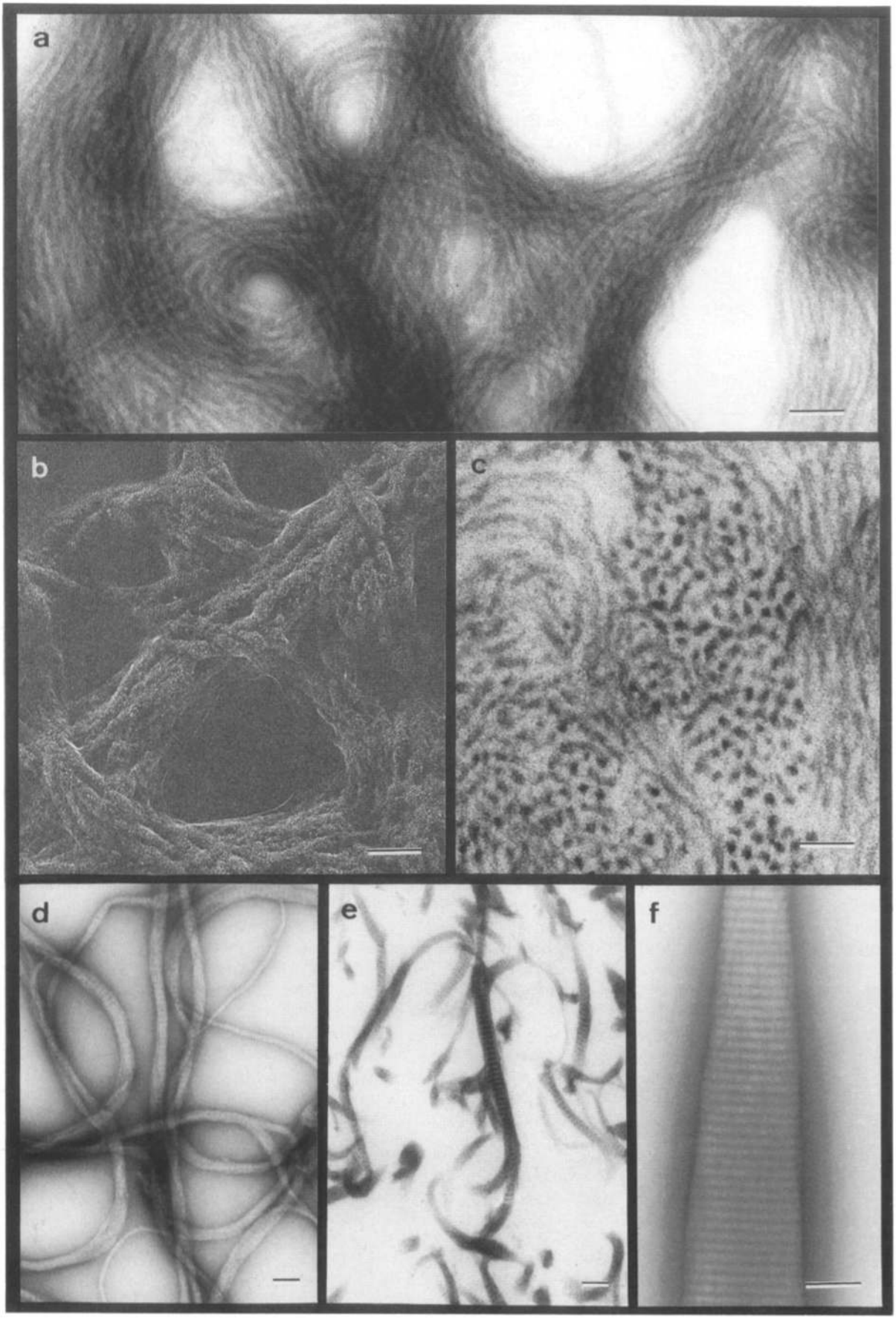
a
b
c
d
e
f

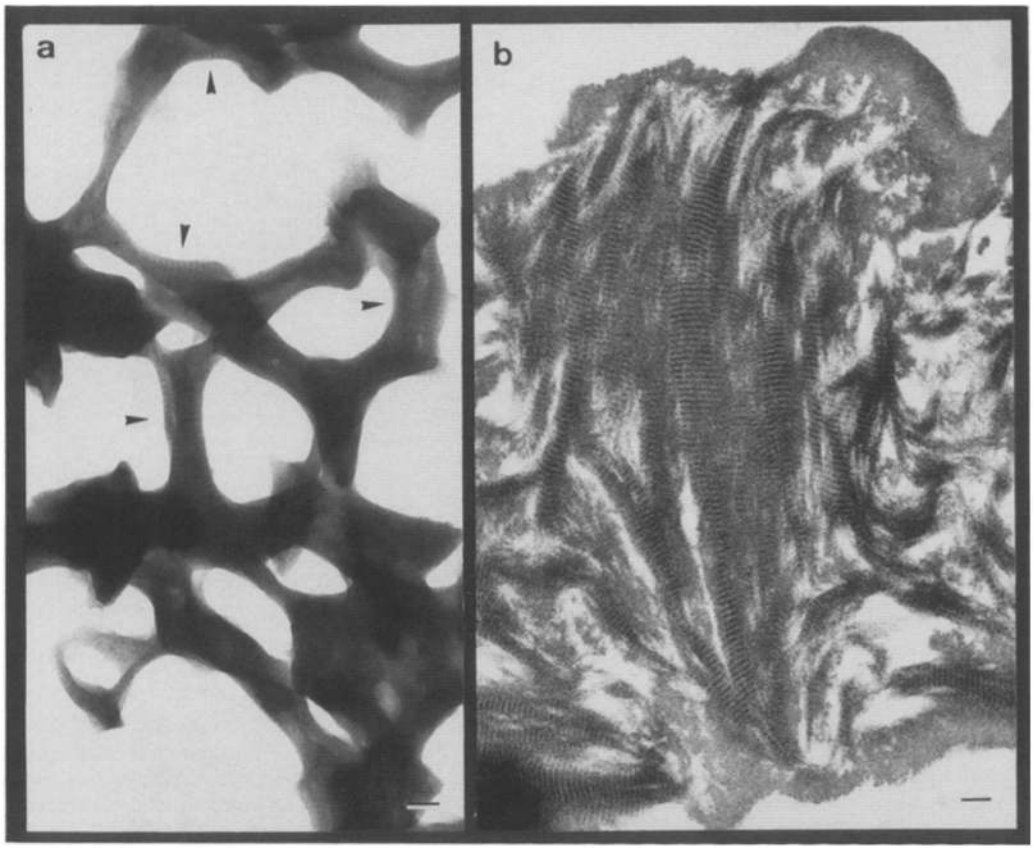

Figure 7. Assembly properties of bacterially expressed mouse NF-L rod domain. Dialysis of urea-solubilized recombinant mouse NF-L rod against 50 mM MES, 1 mM DTT, pH 7.0, containing 20 mM $CaCl_2$ (*a* and *b*) or 20 mM $MgCl_2$ (not shown) for ≥12 h at room temperature produced large, three-dimensional paracrystalline aggregates with an approximate axial periodicity of 21.4 ± 1.5 nm (see Table I). Specimens were prepared by either negative staining (*a*) or plastic embedding/thin sectioning (*b*). Bars, 100 nm (*a* and *b*).

not require an entire 10-nm filament but becomes already manifest with tetrameric protofilaments or octameric protofibrils, provided they involve an N-N or C-C type approximate half-stagger between dimers. In fact, exactly as the periodicity patterns of the tetramer and octamer packing models predict (see Fig. 9 *b*), in some instances alternating shorter (i.e., r_1) and longer (i.e., r_2) axial repeats can be distinguished along protofilaments or protofibrils (see Results and Fig. 8, *a* and *b*).

Whereas the short head-to-tail overlap of dimers gives rise to "bumps" which are accentuated by the presence of the end domains, combination of this longitudinal N-C type overlap with either one of the approximately half-staggered N-N or C-C type lateral interactions of dimers generates "gaps" in the three-dimensional packing of dimers into higher-order oligomers. These bumps and gaps follow the approximate, 21-nm axial periodicity pattern and thereby produce the beaded segments and transverse banding patterns seen in filaments and paracrystalline arrays, respectively.

It must be emphasized that all molecular models for IF structure must be viewed in the framework of an ambiguity of what a bona fide 10-nm filament actually is. MPL measurements using quantitative STEM have provided strong evidence that at least in vitro assembled IFs are polymorphic in the sense that their number of polypeptides per filament cross-section varies both between different as well as along the same filaments (for review see Aebi et al., 1988). Unlike that of actin filaments or microtubules, the IF architecture may not be uniquely specified. This ambiguity may be most pronounced for neurofilaments since despite in vitro assembly of NF-L into 10-nm filaments, in vivo neurofilaments are obligate heteropolymers (Lee et al., 1993; Ching and Liem,

Figure 6. Assembly properties of bacterially expressed tailless mouse NF-L. (*a–c*) Filament bundles obtained after dialysis of urea-solubilized tailless mouse NF-L against 50 mM Hepes, 1 mM DTT, pH 7.5, containing 1 mM $CaCl_2$ for ≥3 h at room temperature. (*d* and *e*) Paracrystalline fibers with an approximate axial periodicity of 20.8 ± 1.1 nm (see Table I) yielded after dialysis of urea-solubilized material against 50 mM Hepes, 1 mM DTT, pH 7.5, containing 10 mM $CaCl_2$ for ≥3 h. (*f*) Paracrystalline arrays with an approximate axial periodicity of 21.2 ± 0.6 nm (see Table I) obtained after dialysis of urea-solubilized material against 50 mM Hepes, 1 mM DTT, pH 7.5, 20 mM $CaCl_2$ for ≥3 h. Specimens were prepared by either negative staining (*a*, *d*, and *f*), glycerol spraying/rotary metal-shadowing (*b*) or plastic embedding/thin sectioning (*c* and *e*). Bars, 100 nm (*a–f*).

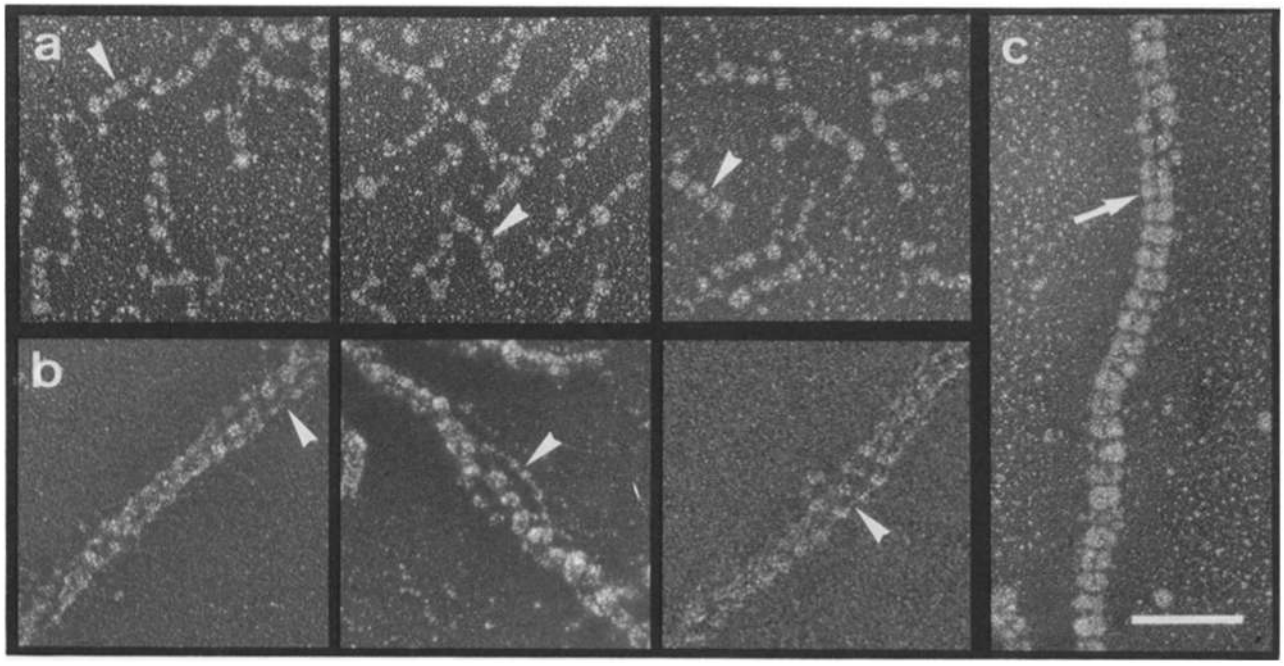

Figure 8. Appearance of the ~21-nm axial beading with NF-L assembly intermediates and unraveling NF-L filaments after glycerol spraying/rotary metal shadowing. (*a*) Examples of small oligomeric particles yielded after dialysis of urea-solubilized NF-L against 5 mM Pipes, 0.1 mM EGTA, 0.1 mM EDTA, 0.1 mMDTT, pH 6.8 at 4°C overnight (Hisanaga et al., 1990). (*b*) Examples of unraveling NF-L filaments in the presence of 10 mM phosphate (Aebi et al., 1983, 1988; Troncoso et al., 1990). (*c*) For comparison, a stretch of an intact NF-L filament is shown. Whereas all examples shown were produced with authentic NF-L, indistinguishable results were obtained with recombinant NF-L (not shown). For the arrowheads and arrow see text. Bar, 100 nm (*a–c*).

1993). How substoichiometric amounts (i.e., <10%) of NF-M or NF-H are incorporated into a neurofilament lattice and thereby affect the filament network remains elusive.

(b) The Roles of the NF-L Head and Tail Domains in 10-nm Filament Assembly

Whereas the headless NF-L fragment yielded 30–50-nm long rod-like particles with a tendency to associate longitudinally into protofilament-like structures (see Fig. 5 *a*) under standard filament forming conditions, the tailless NF-L fragment formed predominantly large structures—possibly aggregates of 10-nm filaments—that adsorbed very poorly to EM grids. Similar to tailless NF-L, the NF-L rod domain also produced large aggregates. While definitely not representing aggregates of 10-nm filaments, most likely, they were made of small, distinct oligomers. In contrast, the rod domains of keratins, desmin, and vimentin form soluble oligomers (e.g., tetramers or octamers) under typical filament forming conditions (e.g., Sauk et al., 1984; Geisler et al., 1992). As formation of similar aggregates was observed after dialysis of the NF-L rod against near-physiological buffer (i.e., at pH 7.5; data not shown), this atypical behavior cannot simply represent isoelectric precipitation of the NF-L rod at pH 6.25.

Upon appropriate adjustment of the assembly conditions (i.e., inclusion of mM amounts of Ca^{2+} or Mg^{2+}) both the headless and tailless NF-L fragments produced filaments, although their morphologies were distinct from that of the 10-nm filaments produced with full-length NF-L. When negatively stained, the filaments formed by headless NF-L appeared thinner (see Table I) and longer than full-length NF-L filaments, whereas after glycerol spraying/rotary metal shadowing they yielded partially unraveled bundles of protofilaments that apparently lacked the 21-nm axial beading diagnostic for bona fide IFs. STEM revealed a MPL corresponding to only 24 truncated—compared to 41 full-length—polypeptides per filament cross-section. In contrast, the negatively stained filaments produced by tailless NF-L appeared wider (see Table I) and more compact than full-length NF-L filaments. In addition, they exhibited a strong tendency to aggregate laterally into bundles. These filaments too lacked the 21-nm axial beading when glycerol-sprayed/rotary metal-shadowed; however, unlike the headless NF-L filaments, they did not unravel into their protofilaments indicating strong lateral interaction. Based on EM and analytical ultracentrifugation in 3–6 M urea, very much like full-length NF-L, the headless, tailless, and rod fragments were competent to form dimers and tetramers (data not shown). Whereas chemical cross-linking has indicated that with desmin the stagger and polarity between dimers is conserved within tetrameric rods, protofilaments and 10-nm filaments (Geisler et al., 1992), it remains to be determined whether this relationship is also conserved among the full-length, headless, tailless, and rod fragments of NF-L.

Taken together, the following roles can be assigned to the two end domains of NF-L during 10-nm filament formation: (*a*) The NH_2-terminal head domain *promotes* lateral association of protofilaments into protofibrils, and ultimately 10-nm filaments, as its removal terminates assembly at the protofilament level. (*b*) In contrast, the COOH-terminal tail domain *controls* lateral assembly of protofilaments so that it

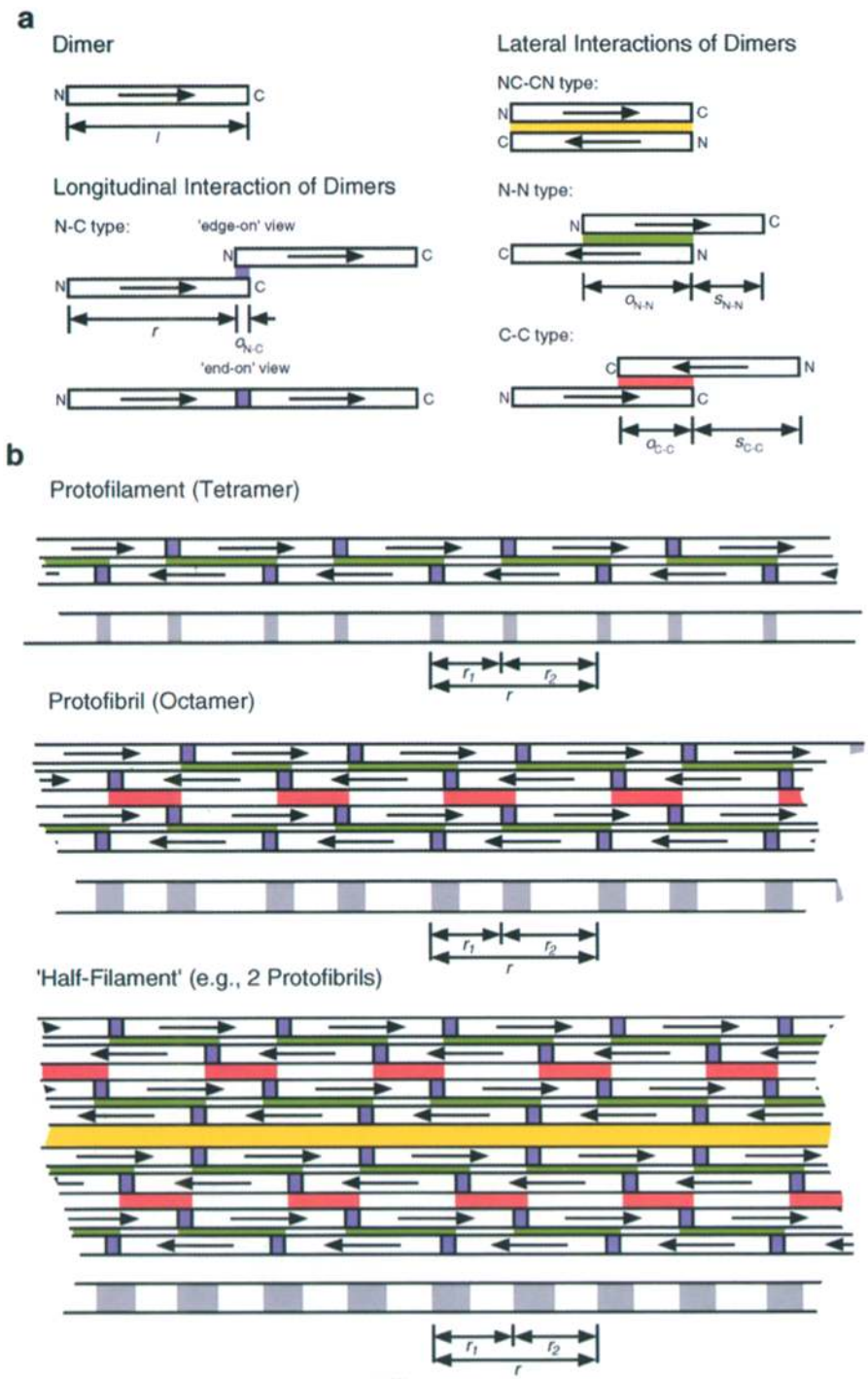

Figure 9. Schematic representation of a molecular model for IF architecture. (*a*) The elementary building block is the dimer rod which consists of two ~40 kD rod domains forming a parallel, unstaggered two-stranded α-helical coiled-coil (i.e., via coils 1A, 1B, 2A, and 2B) with molecular length l. For simplicity, the two end domains have been omitted. Longitudinally, dimers interact head-to-tail with a short, N-C type overlap $o_{N\text{-}C}$, thus yielding an axial repeat $r = l - o_{N\text{-}C}$. Laterally, dimers may interact in three modes to form antiparallel tetramers (e.g., Steinert et al., 1993*a*): (1) in approximate register (i.e., unstaggered) with an NC-CN type overlap; (2) approximately half-staggered with an N-N type overlap $o_{N\text{-}N}$ so as to bring coils 1B into approximate alignment; (3) approximately half-staggered with a C-C type overlap $o_{C\text{-}C}$ so as to bring coils 2B into approximate alignment. Based on chemical cross-linking data, the overlaps for the different modes of dimer–dimer interactions have been calculated for keratin and vimentin IFs (Steinert et al., 1993*a*,*b*,*c*), and for some of those occurring with desmin (Geisler et al., 1992; Geisler, 1993). (*b*) One possible design of protofilaments, protofibrils, and half-filaments sequentially involving the three possible modes of lateral dimer–dimer interactions together with the longitudinal head-to-tail interaction of dimers as defined in *a*. In each case, the "periodicity pattern," i.e., as defined by the N-C type overlap pattern, has also been drawn. Together with the end domains this pattern forms the basis for the 21-nm axial beading seen in filamentous NF-L assemblies (see Fig. 8) as well as the distinct light-dark transverse banding patterns with an approximate, 21-nm axial periodicity depicted in paracrystalline arrays made of truncated NF-Ls (see Fig. 6, *d–f*, and Fig. 7). The choice of the N-N type lateral association of dimers to form the protofilament has been arbitrary, and so has been the combination of N-N and C-C type lateral interactions to produce the protofibril. This becomes evident when trying to delineate protofilaments or protofibrils in the half-filament: there are obviously several possibilities to achieve this.

terminates at the 10-nm filament level, as its removal causes uncontrolled lateral growth and/or aggregation of 10-nm filaments. Hence, the two end domains of NF-L have *antagonistic* effects on the lateral association of protofilaments into higher-order structures, with the effect of the COOH-terminal tail domain being *dominant* over that of the NH_2-terminal head domain. However, as neurofilaments are obligate heteropolymers in vivo (Lee et al., 1993; Ching and Liem, 1993), the actual roles of the NF-L head and tail domains in neurofilament assembly and network formation may be more subtle, as these may be modulated significantly by the presence of NF-M and NF-H.

(c) Differences between Recombinant and Authentic NF-L Filaments May be Due to In Vivo Glycosylation within the NH_2-Terminal Head Domain

Although by standard EM the filaments obtained with

recombinant mouse NF-L appeared indistinguishable from those assembled from authentic bovine NF-L, quantitative STEM revealed their MPLs to differ by roughly eight polypeptides per filament cross-section (see Table I), which as outlined schematically in Fig. 9 *b* corresponds to one octameric protofibril or two tetrameric protofilaments (Eichner et al., 1985; Engel et al., 1985; Aebi et al., 1988; Troncoso et al., 1989). Whereas it is conceivable that this reflects inherent assembly differences between the bovine and mouse NF-L subunits, a more plausible explanation for these assembly differences may be the recent identification of O-glycosidically linked N-acetylglucosamine (O-GlcNAc) monosaccharides to Thr_{21} and Ser_{27} at the NH_2-terminal head domain of NF-L (Dong et al., 1993). These cytoplasmic glycosylations, which are probably reversible in vivo (Kearse and Hart, 1991), occur at a stoichiometry of ~0.1 mole of GlcNAc per mole of authentic NF-L purified from mouse spinal cord. Since bacteria are not known to have comparable glycosylation enzymes, and since in vitro reconstitution experiments with authentic bovine NF-L have shown that the filament morphology, i.e., length and width, critically depends on the assembly conditions (e.g., pH, ionic strength, divalent cations) employed (Aebi et al., 1988; Troncoso et al., 1989), the observed MPL difference between the recombinant and authentic NF-L filaments is most likely due, at least in part, to these glycosidic modifications of the authentic NF-L head domain.

We would like to thank Mr. M. Häner for his untiring help with specimen preparation and electron microscopy. Ms. H. Frefel and Ms. M. Zoller are thanked for their expert photographic work. This project was supported by the Swiss National Science Foundation to U. Aebi, the National Institutes of Health to D. W. Cleveland, and the M. E. Müller Foundation of Switzerland. P. C. Wong has been supported by a postdoctoral fellowship from the Muscular Dystrophy Association.

Received for publication 17 August 1993 and in revised form 23 September 1993.

References

Aebi, U., and T. D. Pollard. 1987. A glow discharge unit to render electron microscope grids and other surfaces hydrophilic. *J. Electron Microsc. Techn.* 7:29–33.

Aebi, U., J. Cohn, L. Buhle, and L. Gerace. 1986. The nuclear lamina is a meshwork of intermediate-type filaments. *Nature (Lond.).* 323:560–564.

Aebi, U., W. E. Fowler, P. Rew, and T.-T. Sun. 1983. The fibrillar substructure of keratin filaments unraveled. *J. Cell Biol.* 97:1131–1143.

Aebi, U., M. Häner, J. Troncoso, R. Eichner, and A. Engel. 1988. Unifying principles in intermediate filament (IF) structure and assembly. *Protoplasma.* 145:73–81.

Albers, K., and E. Fuchs. 1987. The expression of mutant epidermal keratin cDNAs transfected in simple epithelial and squamous cell carcinoma lines. *J. Cell Biol.* 105:791–806.

Albers, K., and E. Fuchs. 1989. Expression of mutant keratin cDNAs in epithelial cells reveals possible mechanisms for initiation and assembly of intermediate filaments. *J. Cell Biol.* 108:1477–1493.

Bader, B. C., T. M. Magin, M. Freudenmann, S. Stumpp, and W. W. Franke. 1991. Intermediate filaments formed de novo from tailless cytokeratins in the cytoplasma and the nucleus. *J. Cell Biol.* 115:1293–1307.

Birkenberger, L., and W. Ip. 1990. Properties of the desmin tail domain studies using synthetic peptides and antipeptide antibodies. *J. Cell Biol.* 111: 2063–2075.

Bonifas, J. M., A. L. Rothman, and E. H. Epstein, Jr. 1991. Epidermolysis bullosa simplex: evidence in two families for keratin gene abnormalities. *Science (Wash. DC).* 254:1202–1205.

Cheng, J., A. J. Syder, Q.-C. Yu, A. Letai, A. S. Paller, and E. Fuchs. 1992. The genetic basis of eidermolytic hyperkeratosis: a disorder of differentiation-specific epidermal keratin genes. *Cell.* 70:811–819.

Chin, S. S. M., P. Macioce, and R. K. H. Liem. 1991. Effects of truncated neurofilament proteins on the endogenous intermediate filaments in transfected cells. *J. Cell Sci.* 99:335–350.

Ching, G. Y., and R. K. H. Liem. 1993. Assembly of type IV neuronal intermediate filaments in nonneuronal cells in the absence of preexisting cytoplasmic intermediate filaments. *J. Cell Biol.* 122:1323–1336.

Chipev, C. C., B. P. Korge, N. Markova, S. J. Bale, J. J. DiGiovanna, J. G. Compton, and P. M. Steinert. 1992. A leucine → proline mutation in the H1 subdomain of keratin 1 causes epidermolytic hyperkeratosis. *Cell.* 70:821–828.

Conway, J. F., and D. A. D. Parry. 1988. Intermediate filament structure: 3. Analysis of sequence homologies. *Int. J. Biol. Macromol.* 10:79–98.

Coulombe, P. A. 1993. The cellular and molecular biology of keratins: beginning a new era. *Curr. Opin. Cell Biol.* 5:17–29.

Coulombe, P. A., and E. Fuchs. 1990. Elucidating the early stages of keratin filament assembly. *J. Cell Biol.* 111:153–169.

Coulombe, P. A., Y.-M. Chan, K. Albers, and E. Fuchs. 1990. Deletions in epidermal keratins leading to alterations in filament organization in vivo and in intermediate filament assembly in vitro. *J. Cell Biol.* 111:3049–3064.

Coulombe, P. A., M. E. Hutton, A. Letai, A. Hebert, A. S. Paller, and E. Fuchs. 1991. Point mutations in human keratin 14 genes of epidermolysis bullosa simplex patients genetic and functional analysis. *Cell.* 66: 1301–1311.

Crewther, W. G., L. M. Dowling, P. M. Steinert, and D. A. D. Parry. 1983. Structure of intermediate filaments. *Int. J. Biol. Macromol.* 5:267–274.

Delacourte, A., G. Filliatreau, F. Boutteau, G. Biserte, and J. Schrevel. 1980. Study of the 10-nm filament fraction during the standard microtubule preparation. *Biochem. J.* 191:543–546.

Dong, D. L.-Y., Z.-S. Xu, M. R. Chevrier, R. J. Cotter, D. W. Cleveland, and G. W. Hart. 1993. Glycosylation of mammalian neurofilaments: localization of multiple O-linked N-acetylglucosamine moieties on neurofilament polypeptides L and M. *J. Biol. Chem.* 268:16679–16687.

Eckelt, A., H. Herrmann, and W. W. Franke. 1992. Assembly of a tailless mutant of the intermediate filament protein, vimentin, in vitro and in vivo. *Eur. J. Cell Biol.* 58:315–330.

Eichner, R., P. Rew, A. Engel, and U. Aebi. 1985. Human epidermal keratin filaments: studies on their structure and assembly. *Ann. NY Acad. Sci.* 455:381–402.

Engel, A., R. Eichner, and U. Aebi. 1985. Polymorphism of reconstituted human epidermal keratin filaments: determination of their mass-per-unit length and width by scanning transmission electron microscopy (STEM). *J. Ultrastruct. Res.* 90:323–335.

Fisher, D. Z., N. Chaudhary, and G. Blobel. 1986. cDNA sequencing of nuclear lamins A and C reveals primary and secondary structural homology to intermediate filament proteins. *Proc. Natl. Acad. Sci. USA.* 83:6450–6454.

Franke, W. W., D. C. Schiller, and C. Grund. 1982. Protofilamentous and annular structures as intermediates during reconstitution of cytokeratin in vitro. *Biol. Cell.* 46:257–268.

Fowler, W., and U. Aebi. 1983. Preparation of single molecules and supramolecular complexes for high-resolution metal shadowing. *J. Ultrastruct. Res.* 83:319–334.

Fuchs, E., and P. A. Coulombe. 1992. Of mice and men: genetic skin disease of keratin. *Cell.* 69:899–902.

Geisler, N. 1993. Chemical crosslinking with disuccinimidyl tartrate defines the relative positions of the two antiparallel coiled coils of the desmin protofilament unit. *FEBS (Fed. Eur. Biochem. Soc.) Lett.* 323(1-2):63–67.

Geisler, N., and K. Weber. 1981. Self assembly *in vitro* of the 68,000 mw component of the mammalian neurofilament triplet protein into intermediate-sized filaments. *J. Mol. Biol.* 151:565–571.

Geisler, N., E. Kaufmann, and K. Weber. 1982. Protein chemical characterization of three structurally distinct domains along the protofilament unit of desmin 10 nm filaments. *Cell.* 30:277–286.

Geisler, N., U. Plessmann, and K. Weber. 1985*a*. The complete amino acid sequence of the major mammalian neurofilament protein (NF-L). *FEBS (Fed. Eur. Biochem. Soc.) Lett.* 182:475–478.

Geisler, N., E. Kaufmann, and K. Weber. 1985*b*. Antiparallel orientation of the two double-stranded coiled-coils in the tetrameric protofilament unit of intermediate filaments. *J. Mol. Biol.* 182:173–177.

Geisler, N., J. Schünemann, and K. Weber. 1992. Chemical cross-linking indicates a staggered and antiparallel protofilament of desmin intermediate filaments and characterizes one higher-level complex between protofilaments. *Eur. J. Biochem.* 206:841–852.

Gieffers, C., and G. Krohne. 1991. In vitro reconstitution of recombinant lamin A and a lamin A mutant lacking the carboxyterminal tail. *Eur. J. Cell Biol.* 55:191–199.

Gill, S. R., P. C. Wong, M. J. Monteiro, and D. W. Cleveland. 1990. Assembly properties of dominant and recessive mutations in the small mouse neurofilament (NF-L) subunits. *J. Cell Biol.* 111:2005–2019.

Gotow, T., M. Takeda, T. Tanaka, and P. H. Hashimoto. 1992. Macromolecular structure of reassembled neurofilaments as revealed by the quick-freeze deep-etch mica method: difference between NF-M and NF-H subunits in their ability to form cross-bridges. *Eur. J. Cell Biol.* 58:331–345.

Hanukoglu, I., and E. Fuchs. 1982. The cDNA sequence of a human epidermal keratin: divergence of sequence but conservation of structure among intermediate filament proteins. *Cell.* 31:243–252.

Hanukoglu, I., and E. Fuchs. 1983. The cDNA sequence of a type II cytoskeletal keratin reveals constant and variable structural domains among keratins. *Cell.* 33:915–924.

Hatzfeld, M., and K. Weber. 1990. Tailless keratins assemble into regular intermediate filaments in vitro. *J. Cell Sci.* 97:317–324.

Hatzfeld, M., and K. Weber. 1991. Modulation of the keratin intermediate filament assembly by single amino acid exchanges in the consensus sequence at the C-terminal end of the rod domain. *J. Cell Sci.* 99:351–362.

Heald, R., and F. D. McKeon. 1990. Mutations of phosphorylation sites in lamin A that prevent nuclear lamina disassembly in mitosis. *Cell.* 61:579–589.

Heitlinger, E., M. Häner, A. Lustig, U. Aebi, and E. A. Nigg. 1991. Expression of chicken lamin B_2 in *E. coli*: characterization of its structure, assembly and molecular interactions. *J. Cell Biol.* 113:485–495.

Heitlinger, E., M. Peter, A. Lustig, W. Villiger, E. A. Nigg, and U. Aebi. 1992. The role of the head and tail domain in lamin structure and assembly: analysis of bacterially expressed chicken lamin A and truncated B_2 lamin. *J. Struct. Biol.* 108:74–91.

Henderson, D., N. Geisler, and K. Weber. 1982. A periodic ultrastructure in intermediate filaments. *J. Mol. Biol.* 155:173–176.

Herrmann, H., I. Hofmann, and W. W. Franke. 1992. Identification of a nonapeptide motif in the vimentin head domain involved in intermediate filament assembly. *J. Mol. Biol.* 223:637–650.

Hisanaga, S., and N. Hirokawa. 1988. Structure of the peripheral domains of neurofilaments revealed by low angle rotary shadowing. *J. Mol. Biol.* 202:297–305.

Hisanaga, S., and N. Hirokawa. 1989. The effects of dephosphorylation on the structure of the projections of neurofilaments. *J. Neurosci.* 9:959–966.

Hisanaga, S., A. Ikai, and N. Hirokawa. 1990. Molecular architecture of the neurofilament. I. Subunit arrangement of neurofilament L protein in the intermediate sized filament. *J. Mol. Biol.* 211:857–869.

Hisanaga, S., and N. Hirokawa. 1990. Molecular architecture of the neurofilament. II. Reassembly process of neurofilament L protein in vitro. *J. Mol. Biol.* 211:871–882.

Hofmann, I., and H. Herrmann. 1992. Interference in vimentin assembly in vitro by synthetic peptides derived from the vimentin head domain. *J. Cell Sci.* 101:687–700.

Ip, W. 1988. Modulation of desmin intermediate filament assembly by a monoclonal antibody. *J. Cell Biol.* 106:735–745.

Ip, W., M. K. Hartzer, Y.-Y. S. Pang, and R. M. Robson. 1985. Assembly of vimentin in vitro and its implications concerning the structure of intermediate filaments. *J. Mol. Biol.* 183:365–375.

Kaufmann, E., K. Weber, and N. Geisler. 1985. Intermediate filament forming ability of desmin derivates lacking either the amino-terminal 67 or the carboxy-terminal 27 residues. *J. Mol. Biol.* 185:733–742.

Kearse, K. P., and G. W. Hart. 1991. Lymphocyte activation induces rapid changes in nuclear and cytoplasmic glycoproteins. *Proc. Natl. Acad. Sci. USA.* 88:1701–1705.

Kouklis, P. D., T. Papamarcaki, A. Merdes, and S. D. Georgatos. 1991. A potential role for the COOH-terminal domain in the lateral packing of type III intermediate filaments. *J. Cell Biol.* 114:773–786.

Lane, E. B., E. L. Rugg, H. Navsaria, I. M. Leigh, A. H. M. Heagerty, A. Ishida-Yamamoto, and R. A. J. Eady. 1992. A mutation in the conserved helix termination peptide of keratin 5 in hereditary skin blistering. *Nature (Lond.).* 356:244–246.

Lee, M. K., Z. Xu, P. C. Wong, and D. W. Cleveland. 1993. Neurofilaments are obligate heteropolymers *in vivo*. *J. Cell Biol.* 122:1337–1350.

Letai, A., P. Coulombe, and E. Fuchs. 1992. Do the ends justify the mean? Proline mutations at the ends of the keratin coiled-coil rod segment are more disruptive than internal mutations. *J. Cell Biol.* 116:1181–1195.

Lewis, S., and N. J. Cowan. 1985. Genetics, evolution, and expression of a 68,000-mol-wt neurofilament protein: isolation of a cloned cDNA probe. *J. Cell Biol.* 100:843–850.

Liem, R. K. H. 1993. Molecular biology of neuronal intermediate filaments. *Curr. Opin. Cell Biol.* 5:12–16.

Liem, R. K. H., and S. B. Hutchison. 1982. Purification of individual components of the neurofilament triplet, filament assembly from the 70,000-dalton subunit. *Biochemistry.* 21:3221–3226.

McCormick, M. B., P. Kouklis, A. Syder, and E. Fuchs. 1993. The roles of the rod end and the tail in vimentin IF assembly and IF network formation. *J. Cell Biol.* 122:395–407.

McKeon, F. D., M. W. Kirschner, and D. Caput. 1986. Homologies in both primary and secondary structure between nuclear envelope and intermediate filament proteins. *Nature (Lond.).* 319:463–468.

McLachlan, A. D., and M. Stewart. 1982. Periodic charge distribution in intermediate filament proteins desmin and vimentin. *J. Mol. Biol.* 162:693–698.

Milam, L., and H. P. Erickson. 1982. Visualization of a 21-nm axial periodicity in shadowed keratin filaments and neurofilaments. *J. Cell Biol.* 94:592–596.

Millonig, G. 1961. A modified procedure for lead staining of thin sections. *J. Biophys. Biochem. Cytol.* 11:736–739.

Moir, R. D., A. D. Donaldson, and M. Stewart. 1991. Expression in *Escherichia coli* of human lamin A and C: influence of head and tail domains on assembly properties and paracrystal formation. *J. Cell Sci.* 99:363–372.

Parry, D. A. D., and P. M. Steinert. 1992. Intermediate filament structure. *Curr. Opin. Cell Biol.* 4:94–98.

Parry, D. A. D., A. C. Steven, and P. M. Steinert. 1985. The coiled-coil molecules of intermediate filaments consist of two parallel chains in exact axial register. *Biochem. Biophys. Res. Commun.* 127:1012–1018.

Potschka, M., R. Nave, K. Weber, and N. Geisler. 1990. The two coiled coils of the isolated rod domain of the intermediate filament protein desmin are staggered. *Eur. J. Biochem.* 190:503–508.

Quinlan, R. A., J. A. Cohlberg, D. C. Schiller, M. Hatzfeld, and W. W. Franke. 1984. Heterotypic tetramer (A2D2) complexes of non-epidermal keratins isolated from cytokeratins of rat hepatocytes and hepatoma cells. *J. Mol. Biol.* 178:365–388.

Quinlan, R. A., M. Hatzfeld, W. W. Franke, A. Lustig, T. Schulthess, and J. Engel. 1986. Characterization of dimer subunits of intermediate filament proteins. *J. Mol. Biol.* 192:337–349.

Raats, J. M. H., F. R. Pieper, W. T. M. Vree Egberts, K. N. Verrijp, F. C. S. Ramaekers, and H. Bloemendal. 1990. Assembly of amino-terminally deleted desmin in vimentin-free cells. *J. Cell Biol.* 111:1971–1985.

Raats, J. M. H., J. B. J. Henderik, M. Verrijp, F. L. G. van Oort, W. L. H. Gerards, F. C. S. Ramaekers, and H. Bloemendal. 1991. Assembly of carboxy-terminally deleted desmin in vimentin-free cells. *Eur. J. Cell Biol.* 56:84–103.

Rothnagel, J. A., A. M. Dominey, L. D. Dempsey, M. A. Longley, D. A. Greenhalgh, T. A. Gagne, M. Huber, E. Frenk, D. Hohl, and D. A. Roop. 1992. Mutations in the rod domains of keratins 1 and 10 in epidermolytic hyperkeratosis. *Science (Wash. DC).* 257:1128–1130.

Sauk, J. J., M. Krumeveide, D. Cocking-Johnson, and J. G. White. 1984. Reconstitution of cryokeratin filaments in vitro: further evidence for the role of nonhelical peptides in filament assembly. *J. Cell Biol.* 99:1590–1597.

Steinert, P. M. 1991*a*. Analysis of the mechanism of assembly of mouse keratin 1/keratin 10 intermediate filaments *in vitro* suggests that intermediate filaments are built from multiple oligomeric units rather than a unique tetrameric building block. *J. Struct. Biol.* 107:175–188.

Steinert, P. M. 1991*b*. Organization of coiled-coil molecules in native keratin 1/keratin 10 intermediate filaments: evidence for alternating rows of antiparallel in-register and antiparallel staggered molecules. *J. Struct. Biol.* 107:157–174.

Steinert, P. M., and D. R. Roop. 1988. Molecular and cellular biology of intermediate filaments. *Annu. Rev. Biochem.* 57:593–625.

Steinert, P. M., and D. A. D. Parry. 1993. The conserved H1 domain of the type II keratin 1 chain plays an essential role in the alignment of the nearest neighbor molecules in mouse and human keratin 1/keratin 10 intermediate filaments at the two- to four-molecule level of structure. *J. Biol. Chem.* 268:2878–2887.

Steinert, P. M., R. H. Rice, D. R. Roop, B. L. Trus, and A. C. Steven. 1983. Complete amino acid sequence of a mouse epidermal keratin subunit and implications for the structure of intermediate filaments. *Nature (Lond.).* 302: 794–800.

Steinert, P. M., L. N. Marekov, R. D. B. Fraser, and D. A. D. Parry. 1993*a*. Keratin intermediate filament structure. Crosslinking studies yield quantitative information on molecular dimensions and mechanism of assembly. *J. Mol. Biol.* 230:436–452.

Steinert, P. M., L. N. Marekov, and D. A. D. Parry. 1993*b*. Conservation of the structure of keratin intermediate filaments: molecular mechanism by which different keratin molecules integrate into pre-existing keratin intermediate filaments during differentiation. *Biochemistry.* 32:10046–10056.

Steinert, P. M., L. N. Marekov, and D. A. D. Parry. 1993*c*. Diversity of intermediate filament structure: evidence that the alignment of coiled-coil molecules in vimentin is different from that of keratin intermediate filaments. *J. Biol. Chem.* In press.

Studier, F. W., and B. A. Moffat. 1986. Use of bacteriophage T7 RNA polymerase to direct selective high-level expression of cloned genes. *J. Mol. Biol.* 189:113–130.

Towbin, H., T. Staehelin, and J. Gordon. 1979. Electrophoretic transfer of proteins from polyacrylamide gels to nitrocellulose sheets: procedure and some applications. *Proc. Natl. Acad. Sci. USA.* 76:4350–4354.

Troncoso, J. C., M. Häner, M. March, J. L. Reichelt, A. Engel, and U. Aebi. 1989. Structure and assembly of specific NF subunit combinations. *In* Springer Series in Biophysics. U. Aebi and A. Engel, editors. 3:33–38.

Troncoso, J. C., J. L. March, M. Häner, and U. Aebi. 1990. Effect of aluminium and other multivalent cations on neurofilaments in vitro: an electron microscopic study. *J. Struct. Biol.* 103:2–12.

Wilson, A. K., P. A. Coulombe, and E. Fuchs. 1992. The roles of K5 and K14 head, tail, and R/KLLEGE domains in keratin filament assembly. *J. Cell Biol.* 119:401–414.

Wong, P. C., and D. W. Cleveland. 1990. Characterization of dominant and recessive assembly defective mutations in mouse neurofilament NF-M. *J. Cell Biol.* 111:1987–2003.

Wrighley, N. 1968. The lattice spacing of crystalline catalase as an internal standard of length in electron microscopy. *J. Ultrastruct. Res.* 24:454–464.